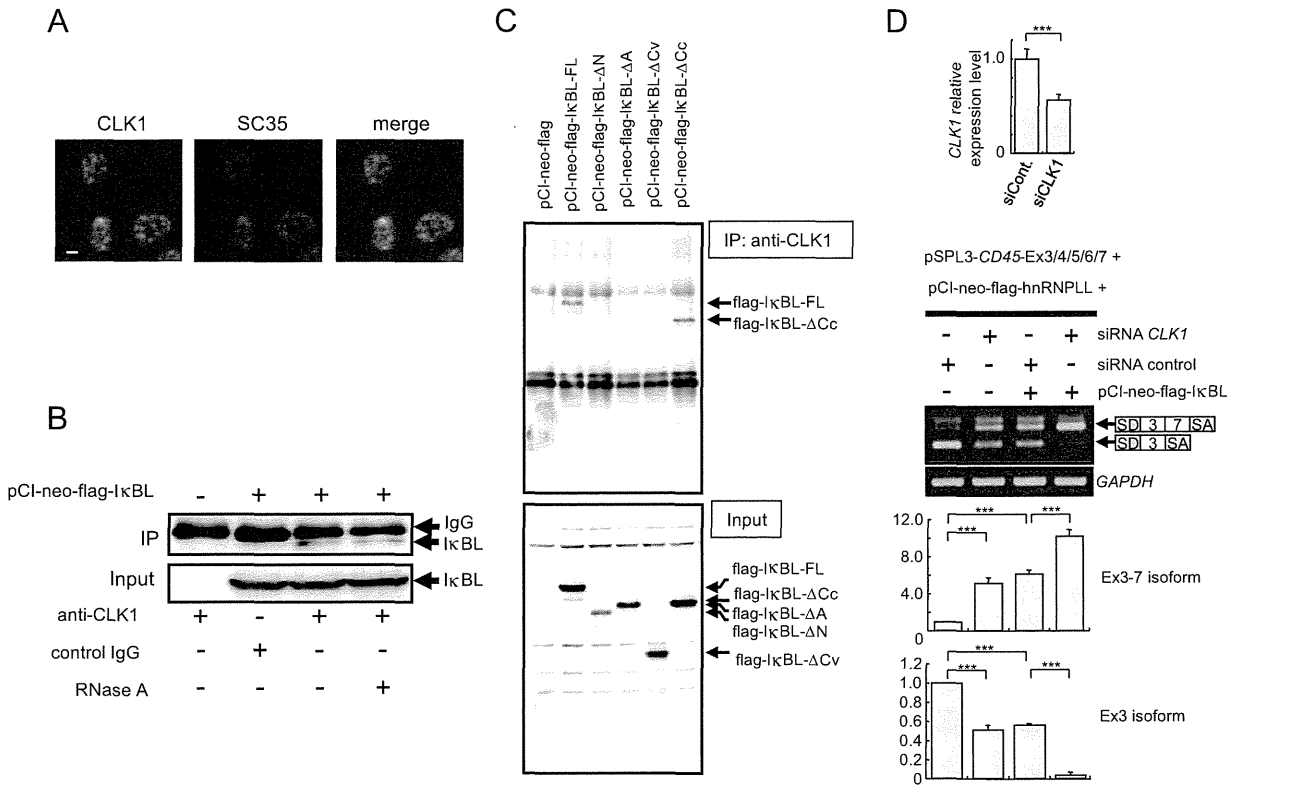

Fig. 3. Interaction of IκBL with CLK1. (A) Subcellular localization of endogenous CLK1 (FITC-labeled, green) and endogenous SC35 (Alexa Fluor 568-labeled, red) were visualized by immunofluorescent staining in HeLa cells. Bar indicates 5 μm. (B) COS7 cells were transfected with or without flag-tagged IκBL, followed by IP using an antibody against CLK1 in the presence or absence of RNase A. The IP products and input lysates were immunoblotted with anti-flag antibody. (C) Co-IP of endogenous CLK1 with flag-IκBL-FL, -ΔN, -ΔA, -ΔCv or -ΔCc. The IP products and input lysates were immunoblotted with anti-flag antibody. The results in (B) and (C) were representatives of three independent experiments. (D) HEK293T cells were treated with siRNA specific to *CLK1*, and then subjected to transfection with *CD45* mini-gene and flag-hnRNPLL with or without flag-IκBL. The transcripts derived from alternative splicing of *CD45* mini-gene were shown. Relative amounts of exons 3-7 isoform and exon 3 isoform were quantified and normalized to *GAPDH* transcripts. Bar graphs represent the quantification of indicated transcripts. Data are shown as means ± SD of four replicates. $^{***}p < 0.005$. (For interpretation of the references to color in this figure legend, the reader is referred to the web version of this article.)

immunoprecipitation with anti-CLK1 antibody, it was found that ASF/SF2 lacking both RRMs failed to associate with CLK1 (Supplementary Fig. S6B and S6C). Because ASF/SF2 was suggested to be involved in the regulation of *CD45* alternative splicing [22–24], we analyzed the hnRNPLL-induced splicing of *CD45* mini-gene in the presence of ASF/SF2-FL or deletion mutant constructs. It was observed that ASF/SF2 inhibited the hnRNPLL-induced exon exclusion of *CD45*. In addition, ASF/SF2 without RRMs lost the inhibitory function, indicating that RRMs of ASF/SF2 were crucial for the regulation of *CD45* alternative splicing (Supplementary Fig. S7).

To investigate the interaction of IκBL with CLK1 and ASF/SF2, we transfected COS7 with EGFP-tagged IκBL in combination with flag-tagged CLK1-FL or deletion constructs. CLK1-FL and CLK1-Δkinase, but not CLK1-ΔN, were co-immunoprecipitated with EGFP-IκBL, indicating that IκBL bound the N-terminal regulatory domain of CLK1 (Fig. 4B). In addition, it was demonstrated that IκBL bound the ASF/SF2 at the RRMs (Fig. 4C). These observations implied that CLK1 and IκBL were competitively associated with RRMs of ASF/SF2.

3.6. Overexpression of IκBL impaired endogenous CD45 alternative splicing in JSL1 T cells

It was reported that a human T cell line, JSL1, expressed a variety of *CD45* isoforms and stimulation with PMA induced the expression of *CD45* transcripts with alternative splicing [25]. We found that steady-state level of mRNA for *NFKBIL1* was significantly reduced in JSL1 treated with PMA (Fig. 5A). To study the effects of IκBL on the endogenous *CD45* alternative splicing, we transfected JSL1 with flag-tagged IκBL followed by a hygromycin selection to obtain a stable cell line expressing IκBL, JSL1-IκBL (Fig. 5B). In comparison with PMA-induced alternative splicing of *CD45* in JSL1, PMA-treated JSL1-IκBL showed a decreased amount of the exons 3-7 isoform and reciprocally increased amount of longer isoforms including the exons 3-5-6-7 isoform (Fig. 5B). Flow cytometry analysis showed that PMA-treated JSL1-IκBL expressed higher amount of CD45RA isoform, that encompassed exon 4, and a slightly lower amount of CD45RO isoform corresponding to the exons 3-7 isoform (Fig. 5C), indicating that IκBL impeded PMA-induced exon exclusions in the alternative splicing of endogenous *CD45*. It also was found that IκBL associated with CLK1 in JSL1-IκBL (Supplementary Fig. S4C).

3.7. IκBL regulates the alternative splicing of influenza A virus M gene

It was reported that a knockdown of *CLK1* reduced the replication of influenza A virus, which was mediated by the impaired alternative splicing of viral *M2* mRNA [26]. To study a possible effect of IκBL on the alternative splicing of influenza *M* gene, we employed a plasmid-based rescue system [27,28]. The plasmid encoding influenza *M* gene was co-transfected with viral RNA polymerase complex constructs into COS7. It was found that IκBL

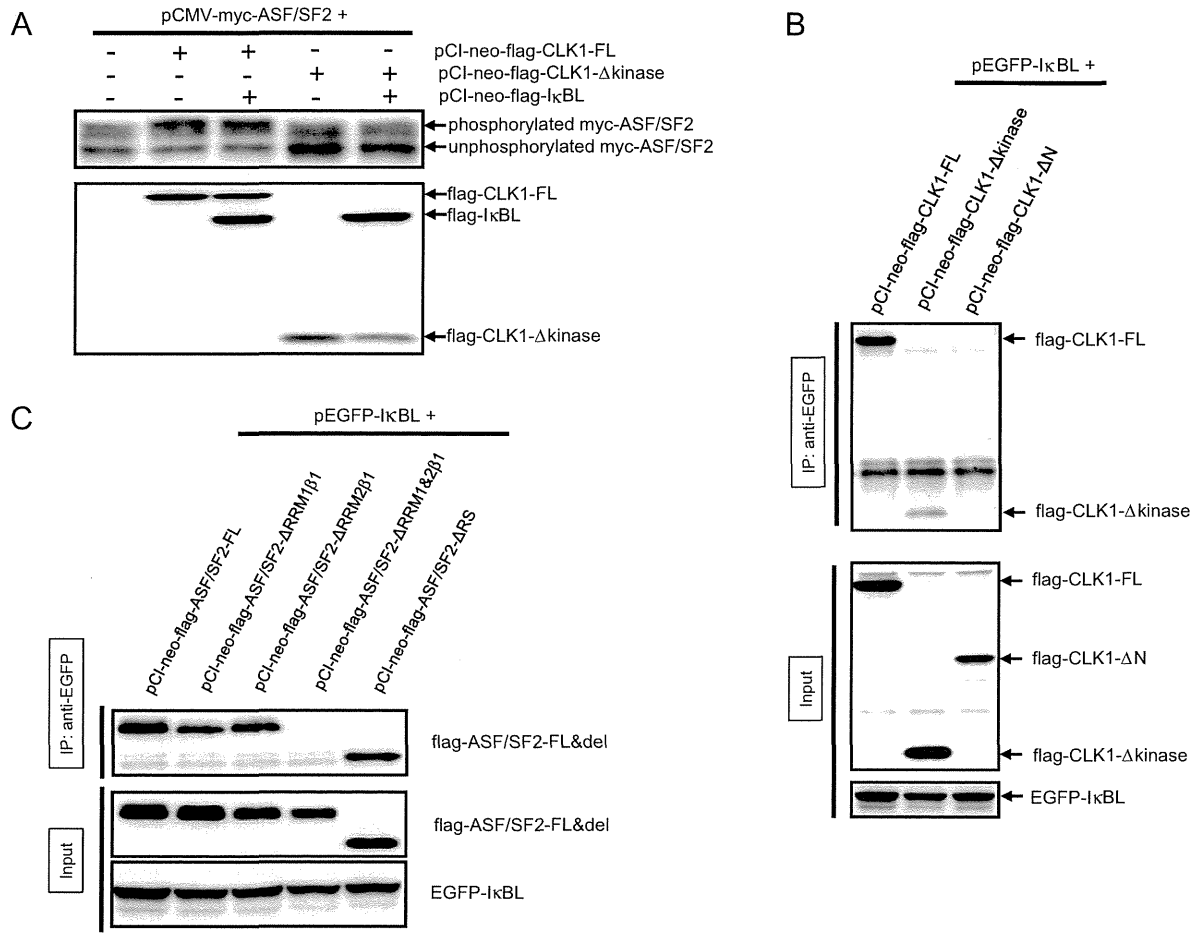

Fig. 4. IκBL did not interfere with CLK1-dependent phosphorylation. (A) COS7 cells were transfected with the constructs of myc-ASF/SF2 along with flag-CLK1-FL or -Δkinase. Immunoblotting showed unphosphorylated and phosphorylated ASF/SF2. In addition, COS7 cells were transfected with flag-IκBL. There was no effect of flag-IκBL on the phosphorylation level of ASF/SF2. (B) Co-IP of EGFP-IκBL with flag-CLK1-FL, Δkinase or -ΔN. (C) Co-IP of EGFP-IκBL with flag-ASF/SF2-FL, -ΔRRM1β1, -ΔRRM2β1, -ΔRRM1&2β1 or -ΔRS. The IP products and input lysates were immunoblotted with anti-flag and anti-EGFP antibodies. The results in (A)–(C) were representatives of three independent experiments.

reduced the amount of *M2* splice variant derived from the *M* gene in a dose-dependent manner (Fig. 6A). On the other hand, the synthesis of *M2* was promoted when *NFKBIL1* expression was interfered by siRNA (Fig. 6B), indicating the role of IκBL in the splicing regulation of viral *M* gene. It was also observed that exogenous expression of ASF/SF2 suppressed the alternative splicing of *M* gene, and this suppression was abolished in the absence RRMs (Supplementary Fig. S8).

4. Discussion

It has been accepted that abnormalities in the regulation of mRNA splicing are tightly linked to the pathogenesis of human disorders in that approximately 15% of the mutations that cause genetic diseases affect pre-mRNA splicing, and splicing mutations might be the most frequent causes of hereditary disease [6,29,30]. In addition, a number of association studies revealed the link of *NFKBIL1* to autoimmune or inflammatory diseases and it has been demonstrated that a sequence variation in the *NFKBIL1* promoter, which results in the reduced expression of IκBL, may confer the susceptibility to RA [4]. Given that IκBL localized in the nuclear speckles and associated with RNA, there is a possible link between the altered expression of IκBL and immune-related diseases via altered RNA splicing.

In this study, it was demonstrated that the exon skipping in alternative splicing of *CD45* was suppressed by IκBL. On the other hand, when the expression of *NFKBIL1* was silenced, the exon skipping of *CD45* was promoted. We also observed that IκBL affected alternative splicing of *CD72* and *CTLA4*. These results strongly indicated that IκBL enhanced exon inclusion in the alternative splicing of immune-related genes. Because *CD45* is expressed in nearly all hematopoietic cells and *CD72* is mainly expressed in B cells, whereas *CTLA4* is known as a surface receptor of T cells, the observations in this study suggested that the regulatory function of IκBL on the alternative splicing was not limited to specific gene or cell type. In addition, the suppressive effects of IκBL were observed in the alternative splicing events induced by hnRNPLL, hnRNPL and FOX1, implying a role of IκBL in a broad context of splicing regulation.

To elucidate the molecular mechanisms of IκBL in the regulation of alternative splicing, we searched for IκBL-interacting proteins using Y2H screening and identified CLK1 to be a binding partner. The association with CLK1 was mediated by N-terminal segment, ankyrin repeat domain segment, and central variable segment of IκBL, all of which were indispensable for IκBL to correctly localize in the nuclear speckles, and to regulate the alternative splicing. These results suggested the involvement of association between IκBL and CLK1 in the alternative splicing.

Although it is not clarified how CLK1 functions on its substrate, it has been reported that CLK1 phosphorylates the SR proteins and plays a role in alternative splicing of target genes including *CLK1* itself [14–16]. In this study, a knockdown of *CLK1* impeded exon

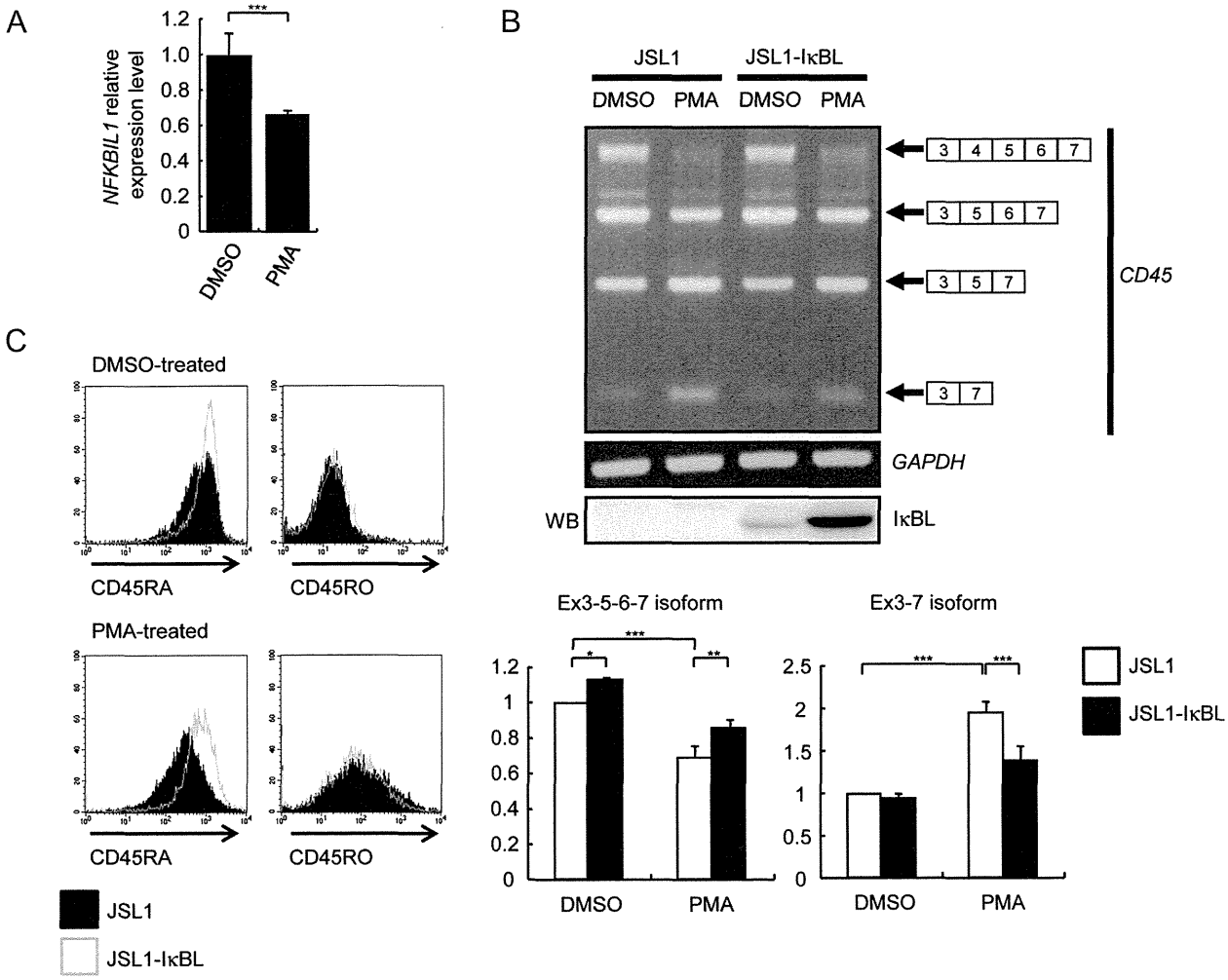

Fig. 5. Role of IκBL in the alternative splicing of endogenous *CD45* in JSL1. (A) Expression of endogenous *NFKBIL1* in JSL1 treated with DMSO (control) or PMA (10 ng/ml, 2 days) was analyzed by using real-time RT-PCR. *NFKBIL1* mRNA level was normalized to 18S rRNA. Data are shown as means ± SD of three replicates. ***$p < 0.005$. (B) RT-PCR analysis showed the alternative splicing of endogenous *CD45* in JSL1 and JSL1-IκBL with DMSO or PMA (10 ng/ml, 2 days) treatment. Relative amounts of exons 3-5-6-7 isoform and exons 3-7 isoform were quantified and normalized to *GAPDH*. Data are shown as means ± SD of three replicates. *$p < 0.05$; **$p < 0.01$; ***$p < 0.005$. (C) Flow cytometry analysis of JSL1 and JSL1-IκBL treated with DMSO or PMA (10 ng/ml, 4 days). PE-labeled CD45RA antibody was used to detect the longer CD45 protein isoforms encompassing exon 4, whereas APC-labeled CD45RO antibody was used to detect the short CD45 protein isoform of exons 3-7.

exclusion, implying that the mechanism by which IκBL regulates alternative splicing might be mediated by functional suppression of CLK1. Although IκBL might interfere with CLK1-induced phosphorylation of SR proteins, we demonstrated in this study that IκBL failed to alter the CLK1-induced phosphorylation of ASF/SF2. To our surprise, it was clearly showed that the functional domain of CLK1 to regulate the alternative splicing of *CD45* was the N-terminal regulatory domain, but not the C-terminal kinase domain. In this context, it is noteworthy that we deciphered a novel mechanism of alternative splicing, where IκBL was involved in, which is independent from the kinase activity of CLK1.

We further investigated the kinase-independent mechanism in the alternative splicing of *CD45*. Our results demonstrated that IκBL bound the N-terminal regulatory domain of CLK1. Albeit that function of the N-terminal domain of CLK1 remained to be clarified, a previous study using Y2H system showed that the N-terminal domain mediated the association with several splicing factors including ASF/SF2, that is one of the most intensively investigated SR proteins [14]. Domain structure of ASF/SF2 is that there are two RRMs followed by a C-terminal RS domain. Each RRM consists of four antiparallel β-strands and two α-helices, which determines the RNA-binding specificity. Importantly, deletion of β1-strand, where RNP submotif locates, is supposed to disrupt the tertiary structure of RRMs. The RS domain includes multiple consecutive phosphorylatable RS/SR dipeptide repeats of which phosphorylation status affects protein–RNA and protein–protein interactions [31,32]. ASF/SF2 plays a pivotal role in the *CD45* alternative splicing [22–24]. In this study, we found that ASF/SF2 counteracted the hnRNPLL-induced *CD45* alternative splicing. Furthermore, it was observed that ASF/SF2 lacking the RRMs, but not RS domain, failed to regulate the *CD45* splicing, which was consistent with that RRMs of ASF/SF2 was indispensable for the alternative splicing [31,32]. We assessed the interaction of IκBL with ASF/SF2, in which IκBL bound the RRMs of ASF/SF2. Therefore, it was supposed that IκBL and CLK1, presumably in a competitive way, interacted with the RRMs of ASF/SF2 to modulate the splicing of *CD45*.

To examine the role of IκBL in alternative splicing of endogenous immune-related genes, JSL1-IκBL, a JSL1 cell line over-expressing flag-IκBL, was established. JSL1-IκBL showed an impeded exon skipping in the PMA-induced alternative splicing of endogenous *CD45*. On the other hand, PMA-induced alternative splicing was accompanied by the reduced expression of endogenous *NFKBIL1*,

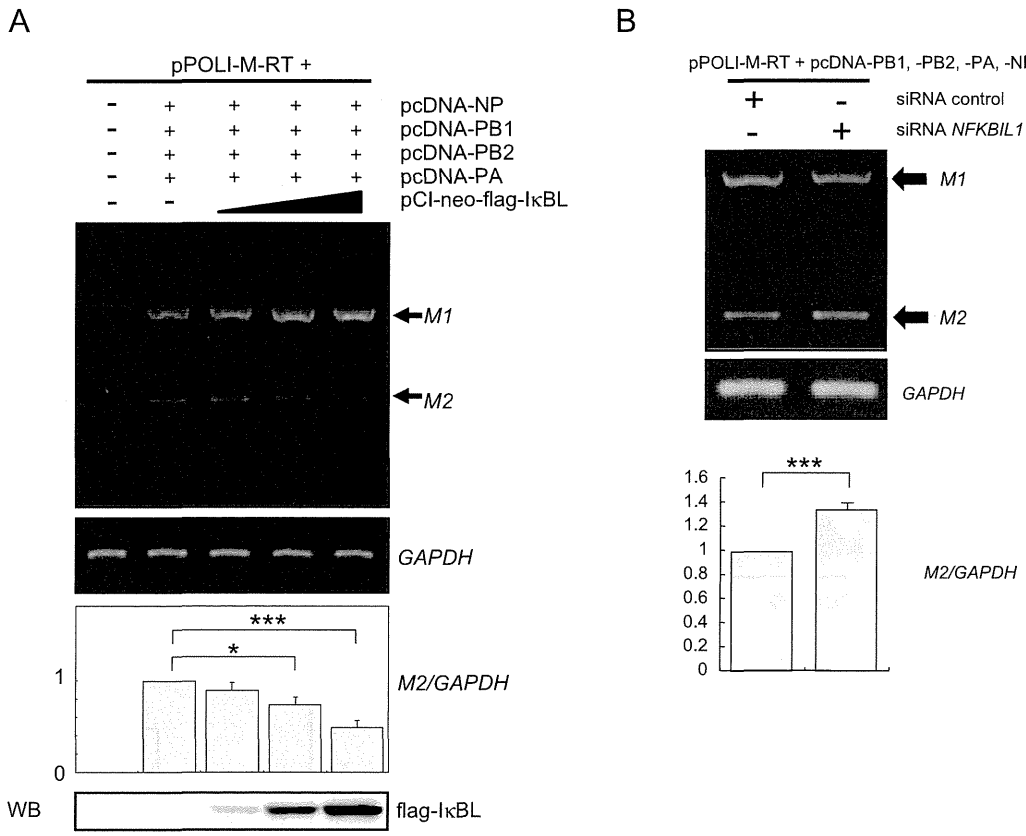

Fig. 6. Regulation of alternative splicing in influenza A virus *M* gene by IκBL. (A) Influenza A virus *M* gene plasmid was co-transfected with plasmids encoding viral RNA polymerase complex factors, i.e. PB1, PB2, PA and NP along with different dose of flag-IκBL into COS7 cells. Expression of flag-IκBL inhibited the generation of spliced *M2* viral RNA in a dose-dependent manner. (B) The effect of *NFKBIL1* knockdown on the alternative splicing of *M* gene was shown. Bar graph indicates the quantification of *M2* viral transcripts normalized to *GAPDH*. Data are shown as means ± SD of three replicates. $^{*}p < 0.05$; $^{***}p < 0.005$.

suggesting that the altered splicing of *CD45* in PMA-stimulated JSL1 was mediated in part by the reduced expression of IκBL. It is well known that abnormally high amount of CD45RO+ T cells predominated in synovial fluid of RA patients [33,34], and our study suggested that the lower expression of IκBL might modulate the activation of T cells and hence would be associated with the susceptibility to RA.

NFKBIL1 is mapped within *HLA*, which comprises a number of genes involved in the protection of host from microorganisms. It has been reported that the knockdown of *CLK1* reduces the replication of influenza A virus, which is associated with the impaired splicing of viral M2 isoform [26]. In this study, it was revealed that IκBL could regulate the level of *M2* RNA transcript, implying that IκBL was capable to inhibit the influenza viral replication. This is a so far unraveled mechanism for fighting against invading microorganisms; by regulating alternative splicing of target viral genes by the *HLA*-linked gene, *NFKBIL1*.

5. Conclusions

IκBL, which interacts with CLK1 and SR proteins in the nuclear speckles, is one of the factors playing crucial roles in the alternative splicing in both human and viral genes. We revealed that IκBL was involved in a novel mechanism for alternative splicing in which CLK1 played a kinase-independent role. The study also provided us with a novel insight into the association of *NFKBIL1* with the susceptibility to inflammatory and/or autoimmune disorders, which is a novel link of *HLA* locus to both immunity and infection in humans, via regulation of alternative splicing.

Author contributions

JA conducted most of the experiments, contributed to data analysis, and wrote the paper. TN participated in the experiments of alternative splicing using mini-genes. TA conducted immunofluorescence staining. HS and MY participated in the Y2H experiment, biochemical study and data analysis. AK designed the study, supervised the experiments, and wrote the paper.

Conflict of interest

The authors declare that they have no conflict of interest.

Acknowledgments

We thank Dr. Kristen W. Lynch (Perelman School of Medicine, University of Pennsylvania) for giving us the JSL1 T cells. We also thank Dr. George G. Brownlee and Dr. Ervin Fodor (Sir William Dunn School of Pathology, University of Oxford) for providing us with the constructs used for plasmid-based rescue system for the influenza A virus. This work was supported by Grants-in-Aids for Scientific Research from the Japan Society for the Promotion of Science and research grants from the Ministry of Health, Labour and Welfare, Japan.

Appendix A. Supplementary data

Supplementary data related to this article can be found at http://dx.doi.org/10.1016/j.jaut.2013.07.010.

References

[1] Allcock RJ, de la Concha EG, Fernandez-Arquero M, Vigil P, Conejero L, Arroyo R, et al. Susceptibility to multiple sclerosis mediated by HLA-DRB1 is influenced by a second gene telomeric of the TNF cluster. Hum Immunol 1999;60:1266–73.

[2] Okamoto K, Makino S, Yoshikawa Y, Takaki A, Nagatsuka Y, Ota M, et al. Identification of I kappa BL as the second major histocompatibility complex-linked susceptibility locus for rheumatoid arthritis. Am J Hum Genet 2003;72:303–12.

[3] Yamashita T, Hamaguchi K, Kusuda Y, Kimura A, Sakata T, Yoshimatsu H. IKBL promoter polymorphism is strongly associated with resistance to type 1 diabetes in Japanese. Tissue Antigens 2004;63:223–30.

[4] Shibata H, Yasunami M, Obuchi N, Takahashi M, Kobayashi Y, Numano F, et al. Direct determination of single nucleotide polymorphism haplotype of NFKBIL1 promoter polymorphism by DNA conformation analysis and its application to association study of chronic inflammatory diseases. Hum Immunol 2006;67:363–73.

[5] Kominami S, Tanabe N, Ota M, Naruse TK, Katsuyama Y, Nakanishi N, et al. HLA-DPB1 and NFKBIL1 may confer the susceptibility to chronic thromboembolic pulmonary hypertension in the absence of deep vein thrombosis. J Hum Genet 2009;54:108–14.

[6] Caceres JF, Kornblihtt AR. Alternative splicing: multiple control mechanisms and involvement in human disease. Trends Genet 2002;18:186–93.

[7] Chen M, Manley JL. Mechanisms of alternative splicing regulation: insights from molecular and genomics approaches. Nat Rev Mol Cell Biol 2009;10:741–54.

[8] Lynch KW. Consequences of regulated pre-mRNA splicing in the immune system. Nat Rev Immunol 2004;4:931–40.

[9] Jacobsen M, Schweer D, Ziegler A, Gaber R, Schock S, Schwinzer R, et al. A point mutation in PTPRC is associated with the development of multiple sclerosis. Nat Genet 2000;26:495–9.

[10] Ueda H, Howson JM, Esposito L, Heward J, Snook H, Chamberlain G, et al. Association of the T-cell regulatory gene CTLA4 with susceptibility to autoimmune disease. Nature 2003;423:506–11.

[11] Semple JI, Brown SE, Sanderson CM, Campbell RD. A distinct bipartite motif is required for the localization of inhibitory kappaB-like (IkappaBL) protein to nuclear speckles. Biochem J 2002;361:489–96.

[12] Greetham D, Ellis CD, Mewar D, Fearon U, an Ultaigh SN, Veale DJ, et al. Functional characterization of NF-kappaB inhibitor-like protein 1 (NFkappaBIL1), a candidate susceptibility gene for rheumatoid arthritis. Hum Mol Genet 2007;16:3027–36.

[13] Lamond AI, Spector DL. Nuclear speckles: a model for nuclear organelles. Nat Rev Mol Cell Biol 2003;4:605–12.

[14] Colwill K, Pawson T, Andrews B, Prasad J, Manley JL, Bell JC, et al. The Clk/Sty protein kinase phosphorylates SR splicing factors and regulates their intranuclear distribution. EMBO J 1996;15:265–75.

[15] Duncan PI, Stojdl DF, Marius RM, Bell JC. In vivo regulation of alternative pre-mRNA splicing by the Clk1 protein kinase. Mol Cell Biol 1997;17:5996–6001.

[16] Muraki M, Ohkawara B, Hosoya T, Onogi H, Koizumi J, Koizumi T, et al. Manipulation of alternative splicing by a newly developed inhibitor of Clks. J Biol Chem 2004;279:24246–54.

[17] Rozas J, Rozas R. DnaSP version 3: an integrated program for molecular population genetics and molecular evolution analysis. Bioinformatics 1999;15:174–5.

[18] Tong A, Nguyen J, Lynch KW. Differential expression of CD45 isoforms is controlled by the combined activity of basal and inducible splicing-regulatory elements in each of the variable exons. J Biol Chem 2005;280:38297–304.

[19] Wu Z, Jia X, de la Cruz L, Su XC, Marzolf B, Troisch P, et al. Memory T cell RNA rearrangement programmed by heterogeneous nuclear ribonucleoprotein hnRNPLL. Immunity 2008;29:863–75.

[20] Oberdoerffer S, Moita LF, Neems D, Freitas RP, Hacohen N, Rao A. Regulation of CD45 alternative splicing by heterogeneous ribonucleoprotein, hnRNPLL. Science 2008;321:686–91.

[21] Rothrock CR, House AE, Lynch KW. HnRNP L represses exon splicing via a regulated exonic splicing silencer. EMBO J 2005;24:2792–802.

[22] Lemaire R, Winne A, Sarkissian M, Lafyatis R. SF2 and SRp55 regulation of CD45 exon 4 skipping during T cell activation. Eur J Immunol 1999;29:823–37.

[23] ten Dam GB, Zilch CF, Wallace D, Wieringa B, Beverley PC, Poels LG, et al. Regulation of alternative splicing of CD45 by antagonistic effects of SR protein splicing factors. J Immunol 2000;164:5287–95.

[24] Motta-Mena LB, Heyd F, Lynch KW. Context-dependent regulatory mechanism of the splicing factor hnRNP L. Mol Cell 2010;37:223–34.

[25] Lynch KW, Weiss A. A model system for activation-induced alternative splicing of CD45 pre-mRNA in T cells implicates protein kinase C and Ras. Mol Cell Biol 2000;20:70–80.

[26] Karlas A, Machuy N, Shin Y, Pleissner KP, Artarini A, Heuer D, et al. Genome-wide RNAi screen identifies human host factors crucial for influenza virus replication. Nature 2010;463:818–22.

[27] Fodor E, Devenish L, Engelhardt OG, Palese P, Brownlee GG, Garcia-Sastre A. Rescue of influenza A virus from recombinant DNA. J Virol 1999;73:9679–82.

[28] Fodor E, Crow M, Mingay LJ, Deng T, Sharps J, Fechter P, et al. A single amino acid mutation in the PA subunit of the influenza virus RNA polymerase inhibits endonucleolytic cleavage of capped RNAs. J Virol 2002;76:8989–9001.

[29] Wang GS, Cooper TA. Splicing in disease: disruption of the splicing code and the decoding machinery. Nat Rev Genet 2007;8:749–61.

[30] Krawczak M, Reiss J, Cooper DN. The mutational spectrum of single base-pair substitutions in mRNA splice junctions of human genes: causes and consequences. Hum Genet 1992;90:41–54.

[31] Zuo P, Manley JL. Functional domains of the human splicing factor ASF/SF2. EMBO J 1993;12:4727–37.

[32] Caceres JF, Krainer AR. Functional analysis of pre-mRNA splicing factor SF2/ASF structural domains. EMBO J 1993;12:4715–26.

[33] Mamoune A, Durand V, Le Goff P, Pennec YL, Youinou P, Le Corre R. Abnormal distribution of CD45 isoforms expressed by CD4+ and CD8+ T cells in rheumatoid arthritis. Histol Histopathol 2000;15:587–91.

[34] Matthews N, Emery P, Pilling D, Akbar A, Salmon M. Subpopulations of primed T helper cells in rheumatoid arthritis. Arthritis Rheum 1993;36:603–7.

PLOS ONE

High Resolution Crystal Structure of the Grb2 SH2 Domain with a Phosphopeptide Derived from CD28

Kunitake Higo[1], Teikichi Ikura[2], Masayuki Oda[3], Hisayuki Morii[4], Jun Takahashi[1], Ryo Abe[1], Nobutoshi Ito[2]*

1 Research Institute for Biomedical Sciences, Tokyo University of Science, Noda-shi, Chiba, Japan, **2** Medical Research Institute, Tokyo Medical and Dental University, Bunkyo-ku, Tokyo, Japan, **3** Graduate School of Life and Environmental Sciences, Kyoto Prefectural University, Sakyo-ku, Kyoto-shi, Kyoto, Japan, **4** Biomedical Research Institute, National Institute of Advanced Industrial Science and Technology, Tsukuba-shi, Ibaraki, Japan

Abstract

Src homology 2 (SH2) domains play a critical role in cellular signal transduction. They bind to peptides containing phosphotyrosine (pY) with various specificities that depend on the flanking amino-acid residues. The SH2 domain of growth-factor receptor-bound protein 2 (Grb2) specifically recognizes pY-X-N-X, whereas the SH2 domains in phosphatidylinositol 3-kinase (PI3K) recognize pY-X-X-M. Binding of the pY site in CD28 (pY-M-N-M) by PI3K and Grb2 through their SH2 domains is a key step that triggers the CD28 signal transduction for T cell activation and differentiation. In this study, we determined the crystal structure of the Grb2 SH2 domain in complex with a pY-containing peptide derived from CD28 at 1.35 Å resolution. The peptide was found to adopt a twisted U-type conformation, similar to, but distinct from type-I β-turn. In all previously reported crystal structures, the peptide bound to the Grb2 SH2 domains adopts a type-I β-turn conformation, except those with a proline residue at the pY+3 position. Molecular modeling also suggests that the same peptide bound to PI3K might adopt a very different conformation.

Citation: Higo K, Ikura T, Oda M, Morii H, Takahashi J, et al. (2013) High Resolution Crystal Structure of the Grb2 SH2 Domain with a Phosphopeptide Derived from CD28. PLoS ONE 8(9): e74482. doi:10.1371/journal.pone.0074482

Editor: Jon C.D. Houtman, University of Iowa, United States of America

Received May 30, 2013; **Accepted** August 1, 2013; **Published** September 30, 2013

Funding: This work was in part supported by JSPS KAKENHI Grant Number 20159453 (http://www.jsps.go.jp/english/). The funders had no role in study design, data collection and analysis, decision to publish, or preparation of the manuscript.

Competing Interests: The authors have declared that no competing interests exist.

* E-mail: ito.str@tmd.ac.jp

Introduction

Src homology 2 (SH2) domains are critical components of intracellular proteins that promote signal transduction. SH2 domains recognize phosphotyrosine (pY)-containing sequences in proteins. Growth-factor receptor-bound protein 2 (Grb2) is an adaptor protein that has an SH3-SH2-SH3 domain architecture [1]. The Grb2 SH2 domain mediates activation of the Ras pathway through binding to phosphotyrosyl motifs on either growth factor receptors such as epidermal growth factor receptor or other adaptor proteins such as Shc [2]. Grb2 SH2 specifically binds to the pY-X-N-X consensus sequence where X is any amino acid; however, it binds to pY-(L/V)-N-(V/P) with higher affinity [3,4]. The selective inhibition of Grb2 SH2 binding to phosphorylated proteins is expected to be useful for the prevention of hyperproliferative diseases.

Three-dimensional structures of Grb2 SH2 in complex with peptides containing pY determined at atomic resolution can be useful for inhibitor development, and several such structures have been reported [4–7]. These studies showed that peptides bound to Grb2 SH2 typically adopt a type-I β-turn conformation.

Ligand binding to the CD28 receptor on the T cell surface is a costimulatory signal that acts, along with recognition of the antigen-major histocompatibility complex by the T cell receptor, to trigger full T cell activation and differentiation into effector T cells [8]. A number of signaling molecules such as Grb2 and phosphatidylinositol 3-kinase (PI3K) bind to the cytoplasmic region of CD28 and activate CD28-mediated costimulatory signaling [9,10]. These molecules bind to CD28 via their SH2 domains primarily to the sequence pY-M-N-M. The consensus Grb2 SH2-binding sequence is pY-X-N-X, whereas the PI3K SH2-binding consensus sequence is pY-X-X-M. CD28 contains the sequence pY-M-N-M in its cytoplasmic region, which enables it to bind both Grb2 SH2 and PI3K SH2 [9]. However, little is known about the molecular details of these interactions.

In this study, we report the crystal structure of Grb2 SH2 in complex with a CD28-derived peptide consisting of 8 amino acids, including the pY-M-N-M sequence, at a resolution of 1.35 Å. This is the first report of the structure of CD28 bound to Grb2 SH2. The high-resolution structure revealed that the bound peptide adopts a conformation similar to, but distinct from the canonical type-I β-turn. Such deviations might exist in other Grb2 SH2/peptide complexes. The possibility that this same peptide adopts a very different conformation when bound to PI3K SH2 is also discussed.

Materials and Methods

Expression and purification of the Grb2 SH2 domain

The SH2 domain of human Grb2 (residues 60–152) was expressed in *Escherichia coli* Bl21(DE3) cells as a glutathione *S*-transferase (GST)-fusion protein using the pGEX-4T-1 vector (GE Healthcare) in LB medium containing 100 μg/mL ampicillin. Protein expression was induced with 0.1 mM isopropyl β-D-1-

Table 1. Statistics for data collection and structure refinement.

Data collection	
Spacegroup	$P6_122$
Unit cell parameters	
a, *b*, *c* (Å)	59.0, 59.0, 117.1
Resolution (Å)	50–1.35 (1.37–1.35) *
R_{sym}	0.057 (0.498)
Completeness (%)	97.7 (98.4)
Redundancy	20.6 (21.2)
Refinement	
Resolution (Å)	50–1.35
Number of reflections	26430
R_{work}/R_{free}	0.176/0.209
Number of non-hydrogen atoms	938
(Protein atoms)	869
(Ion atoms)	5
(Water atoms)	64
RMS deviations from ideal values	
Bond length (Å)	0.020
Bond angles (degree)	2.106
Average B-factor of protein atoms (Å^2)	19.0

*Values shown in parentheses are for the highest-resolution shell.
doi:10.1371/journal.pone.0074482.t001

thiogalactopyranoside (IPTG) at 20°C, and the culture was grown for 12 hours. For Grb2 SH2 protein purification, the *E. coli* cell pellet was suspended in lysis buffer (50 mM Tris HCl [pH 8.0] and 150 mM NaCl) and sonicated on ice. After centrifugation, the supernatant was applied to glutathione sepharose 4B beads (GE Healthcare) and eluted with elution buffer (20 mM Tris HCl [pH 8.0], 200 mM NaCl, 500 μM dithiothreitol (DTT), and 10 mM reduced glutathione). The GST protein was separated from Grb2 SH2 by proteolytic cleavage with thrombin (at room temperature, overnight). The Grb2 SH2 protein was further purified by anion-exchange chromatography with a NaCl gradient (0–1.0 M NaCl in 20 mM Tris HCl [pH 8.0]) and gel-filtration chromatography at 4°C. Finally, the purified Grb2 SH2 protein was concentrated to 5 mg/mL in 20 mM Tris HCl (pH 8.0) and 100 mM NaCl.

Synthesis of the CD28-derived peptide

The 8-residue phosphopeptide, S-D-pY-M-N-M-T-P, which corresponds to residues 189–196 of human CD28, was synthesized by the Fmoc solid-phase method with a PSSM8 peptide synthesizer (Shimadzu Corp.). The C-terminus is a carboxyamide group prepared with Fmoc-NH-SAL-PEG resin (Watanabe Chemicals). Phosphorylated tyrosine was incorporated at the specific position by using *O*-monobenzyl-protected Fmoc-phosphotyrosine (Fmoc-Tyr(PO(OBzl)OH)-OH) [11]. After completion of chain-elongation, the products were cleaved using a mixture of trifluoroacetic acid, 1,2-ethanedithiol, tri-isopropyl silane, and water (86:6:6:2). The peptides were precipitated with diethyl ether, purified by reverse-phase HPLC using YMC-Pack-Pro-C18 column (YMC Co., Ltd.), and verified by mass spectrometry (Shimadzu QP-8000α). Phosphorylation was confirmed by an 8-nm blue shift of the absorption band for tyrosine.

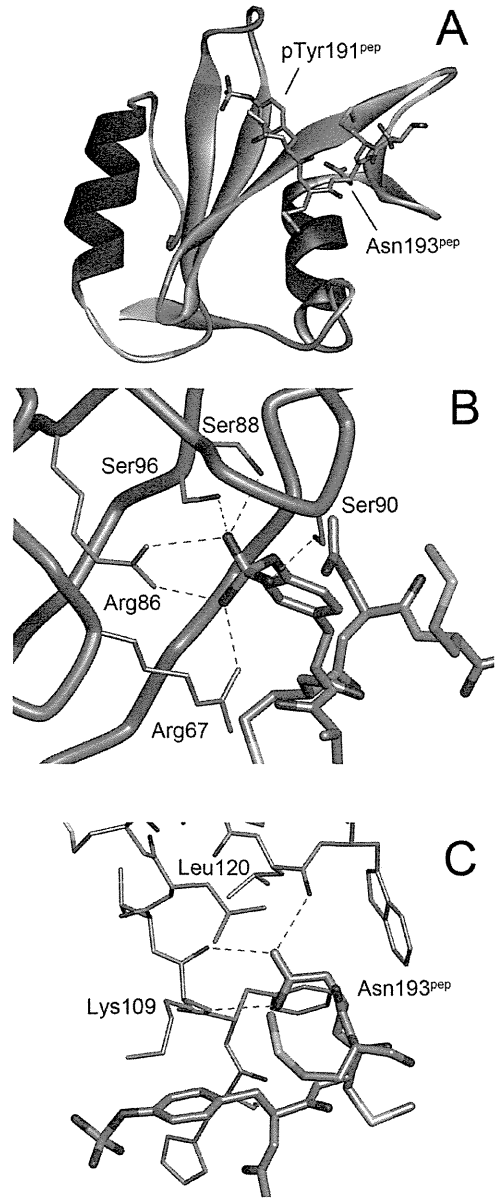

Figure 1. The structure of the Grb2 SH2 domain in complex with a CD28-derived peptide. (A) The overall structure. Grb2 SH2 is shown as a cartoon model, whereas the peptide is shown as a stick model. (B) The interactions between the phosphotyrosine, pTyr191^{pep}, and the SH2 domain. The main-chain trace of the SH2 domain is shown as blue tubes with the side-chains of some key residues in thin sticks. The phosphopeptides are shown as thick stick models. The green dashed lines indicate hydrogen bonds. (C) The interactions between the conserved asparagine, Asn193^{pep}, of the peptide (thick sticks) and the SH2 domain (thin sticks).
doi:10.1371/journal.pone.0074482.g001

Crystallization of the Grb2 SH2/CD28 peptide complex

The crystals of the Grb2 SH2/CD28 peptide complex were obtained by the hanging-drop method. Initial screening was performed with Crystal Screen and Crystal Screen 2 (Hampton Research Inc.), which produced small crystals. After refining the conditions, rod-like crystals, up to 200 μm long, were obtained in 100 mM HEPES (pH 7.5), 1.25 M sodium acetate, and 100 mM cadmium sulfate.

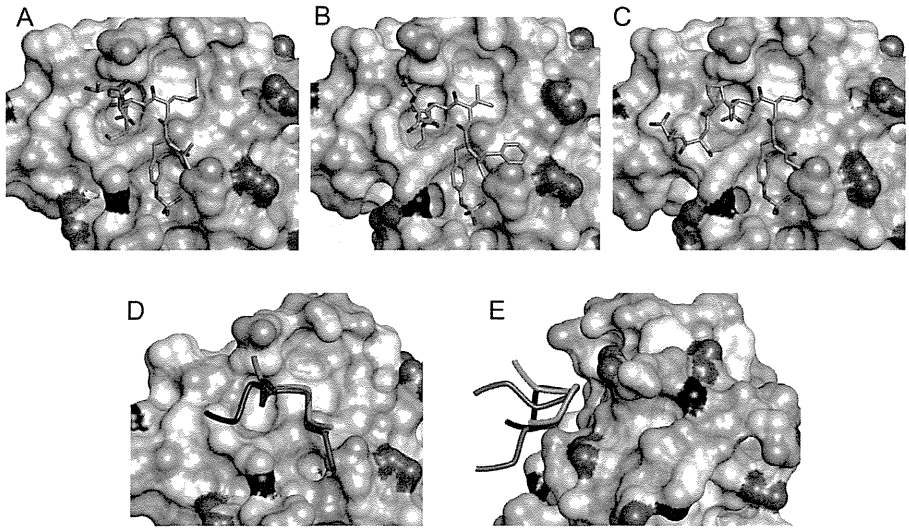

Figure 2. Comparison of the structures of phosphopeptides bound to Grb2 SH2. (A) CD28 (present work, D-pY-M-N-M-T). (B) BCR-Abl (a typical type-I β-turn, PDB ID: 1BMB, F-pY-V-N-V-E) (C) AICD (with a Pro residue at the pY+3 position, PDB ID: 3MXC, G-pY-E-N-P-T-Y). The SH2 domains are shown as surface models, whereas the phosphopeptides are shown as stick models. The thin green lines indicate the distance between the main-chain O of pY and the main-chain N of pY+3, which form a hydrogen bond in the type-I β-turn. The side-chains of some flanking residues are missing due to their weak electron density. (D) Superposition of the 3 peptides. The tubes represent the main-chain traces of CD28 (green), BCR-Abl (red), and AICD (blue). (E) Superposition of CD28, BCR-Abl, and AICD as in (D) but vertically rotated by approximately 90°.
doi:10.1371/journal.pone.0074482.g002

Data collection, structure determination, and refinement

Diffraction data was collected from a single crystal at Beamline NW12A of the Photon Factory (Tsukuba, Japan) at 100K. The diffraction data were integrated and scaled using HKL2000 (HKL Research Inc.). The space group was $P6_122$ ($a = 59.0$ Å, $b = 59.0$ Å, $c = 117.1$ Å) and the asymmetric unit contained a single Grb2 SH2/CD28 peptide complex.

Structure determination and refinement was performed using the CCP4 suite [12]. The structure was solved with PHASER [13] by molecular replacement using another previously reported Grb2 SH2 structure [14]. The structure was refined using REFMAC [15] with restrained anisotropic temperature factors. The graphics program Coot was used for model building [16]. In the last cycle of the refinement, the positional restraints for the phosphotyrosine side-chain were removed to allow the diffraction data to determine its structure. The figures were prepared using Discovery Studio (Accelrys Inc.) and Molscript [17].

Some statistics for data collection and structure refinement are shown in Table 1. The coordinates and structural data for the complex have been deposited in the Protein Data Bank (PDB ID: 3WA4).

Table 2. Main-chain torsion angles (φ/ψ) of the phosphopeptide bound to the Grb2 SH2 domain and their amino acid sequences[a].

PDB ID	Resolution (Å)	pY+1	pY+2 [N]	pY+3	O–N distance[b] (Å)
1BMB	1.8	−52.9/−33.4 [V]	−99.6/14.2	[V]	3.03
1BM2	2.1	−58.9/−44.5 [V]	−83.0/−12.6	[V]	3.22
1JYR	1.55	−59.0/−32.3 [V]	−103.8/14.9	[V]	3.11
1TZE	2.1	−54.9/−28.9 [V]	−103.2/12.8	[V]	3.02
1ZFP	1.8	−61.8/−43.4 [I]	−88.0/19.8	[Q]	3.37
3N8M	2.0	−52.4/−35.0 [V]	−100.7/10.9	[V]	3.07
CD28[c]	1.35	−72.7/−21.5 [M]	−103.6/39.8	[M]	3.71
β-turn[d]	–	−60/−30	−90/0	–	–
3MXC	2.0	−67.3/−32.9 [E]	−99.2/127.0	[P]	5.10
3MXY	2.3	−60.6/−40.3 [V]	−92.8/142.8	[P]	5.11

[a]The angles are given in degree. The residues in the pY+1 and pY+3 positions are shown as one-letter codes in square brackets.
[b]The distance between the main-chain O of pY and the main-chain N of pY+3, which form a hydrogen bond in type-I β-turn.
[c]The structure reported in this work.
[d]Theoretically idealized values for type-I β-turn.
doi:10.1371/journal.pone.0074482.t002

Results

In general, the folds of the Grb2 SH2 domain were essentially the same as those previously reported; consisting of a central, antiparallel β-sheet flanked by 2 α-helices (Fig. 1A) [4–7]. The conformation of Trp121 of Grb2 SH2 was the same as other peptide-bound structures with a χ_1 rotation of approximately 120° compared to the peptide-free structure [7]. The phosphorylated CD28 peptide binds to the Grb2 SH2 recognition site across the exposed edge of the central β-sheet. The phosphotyrosine is located between the β-sheet and the amino-terminal α-helix, and is recognized by a number of residues (Fig. 1B&C). The phosphate moiety of the phosphotyrosine (pTyr191^{pep}, the amino acid residues of the CD28-derived peptide are denoted with a "pep" suffix hereafter) directly interacts with the side chains of Arg67, Arg86, Ser88, Ser90, and Ser96. The side-chain of Asn193^{pep} at the pY+2 position forms a pair of hydrogen bonds with the main-chain amide and carbonyl groups of Lys109. Another hydrogen bond is observed between $N_{\delta 2}$ of Asn193^{pep} and the main-chain O of Leu120. These interactions involving the conserved pTyr and Asn have also been observed in other Grb2/peptide complexes [4–7].

The 2 methionine residues, which are unique to the CD28-derived peptide, appear to contribute to the binding mainly through hydrophobic interactions. The side chain of Met192^{pep}, at

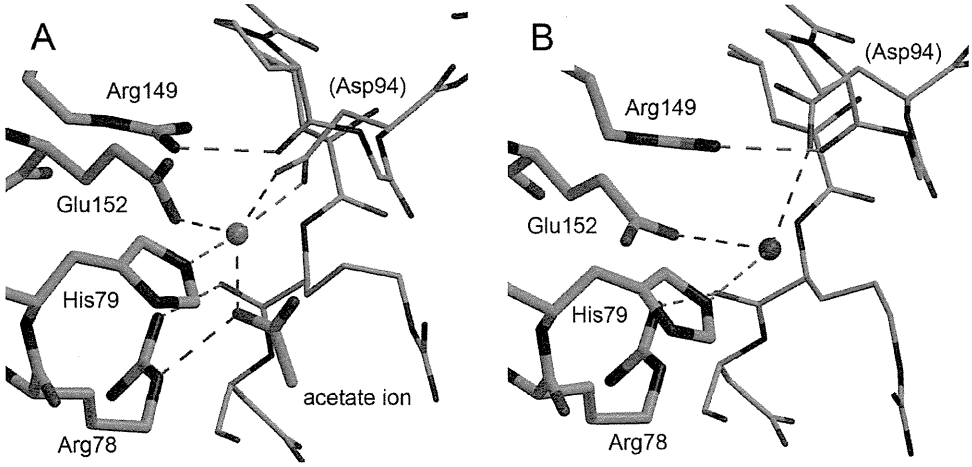

Figure 3. The cadmium binding site. (A) The cadmium binding site located between 2 neighboring molecules in the crystal. The cadmium ion is shown as a green sphere. The Grb2 SH2 molecule is shown in thick lines, whereas a symmetrically-related molecule is shown in thin lines. Green dashed lines indicated the coordinate and hydrogen bonds. (B) The corresponding site in Grb2 SH2/AICD (PDB ID: 3MXC). The red sphere represents a water molecule.
doi:10.1371/journal.pone.0074482.g003

the pY+1 position, is close to the benzene ring of Phe108 and the alkyl of Gln106. The side chain of Met194^{pep}, at the pY+3 position, interacts with Leu111 and Lys109 as well as the phosphotyrosine, although these interactions seem weaker than those of Met192^{pep} as suggested by their higher temperature factors (the average temperature factors of the side chain atoms are 27.0 Å^2 and 38.6 Å^2 for Met192^{pep} and Met194^{pep}, respectively).

The peptide adopts a bent conformation similar to the type-I β-turn, which is the canonical conformation of peptides bound to Grb2 SH2 [5,18,19]. However, the hallmark hydrogen bond between the main-chain oxygen of pY and the main-chain nitrogen of the pY+3 residue (Met194^{pep} in our structure) is not formed (Fig. 2A). Not only are they separated by greater than 3.7 Å, but the direction of the N-H bond, assuming an ordinary structure for the amide group, does not point toward the carbonyl oxygen, making the presence of the hydrogen bond unlikely. Comparison of the main-chain torsion angles φ and ψ shows that the difference between this structure and the type-I β-turn is mainly caused by the ψ angle of the conserved Asn residue at pY+2 (Table 2). In type-I β-turns, this angle should be close to 0°; however, in our structure, it is approximately 40°. Consequently, the CD28-derived peptide is slightly lifted away from Grb2 SH2, making it a more "twisted" conformation than a canonical type-I β-turn (Fig. 2D). This twist also creates more space between the peptide and the protein, and accommodates the side chain of Met194^{pep}.

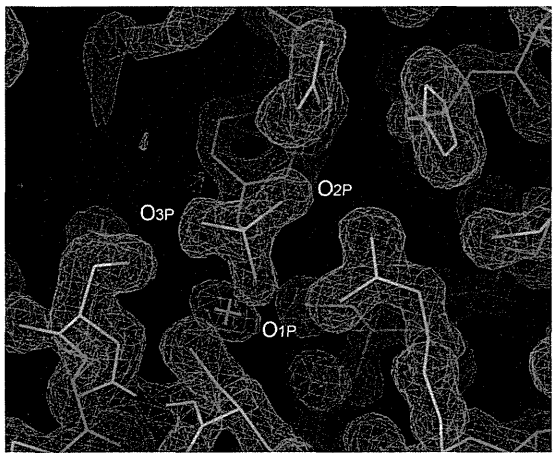

Figure 4. The 2Fo–Fc map around the phosphate group of the phosphotyrosine residue, pTyr191^{pep}. The contour level is set to 1.2 σ, where σ is the root-mean-square deviation of the electron density.
doi:10.1371/journal.pone.0074482.g004

A very strong electron density, which was interpreted as a cadmium ion, was observed between 2 molecules in the crystal lattice. This ion is coordinated by the Nε_2 of His79 and a carboxyl oxygen of Glu152 of one Grb2 molecule and 2 carboxyl oxygens of Asp94 in a neighboring molecule. An acetate ion, which was required for the crystallization, also coordinated to it (Fig. 3A).

In our crystallization trials, the addition of cadmium sulfate markedly improved the appearance and diffraction quality of the crystals. Among the previously reported Grb2 SH2 crystal structures, 2 (PDB ID: 3MXC and 3MXY) have the same space groups and similar unit cell parameters as our structure [20]. These 2 structures are Grb2 SH2/amyloid precursor intracellular C-terminal domain (AICD)-derived peptide structures. A comparison of these Grb2 SH2/AICD structures with ours revealed that their crystal packing is very similar. Yet the resolutions of the Grb2 SH2/AICD 2 structures, 2.0 Å and 2.3 Å, are much lower than that of our structure at 1.35 Å. In these other structures, the cadmium binding site is occupied by a water molecule that forms some hydrogen bonds (Fig. 3B). The presence of the cadmium ion appears to have increased the number of polar interactions between the 2 molecules. It may also have contributed to the improved crystal quality by replacing the intermolecular network of hydrogen bonds with stronger coordinate bonds.

The high resolution of the structure presented here allowed us to determine the geometry of the phosphotyrosine in detail (Fig. 4 & Table 3). In the very last cycle of the structure refinement, the positional constraints for the side-chain atoms of the phosphotyrosine were removed to make the most of the experimental data and investigate its geometry. Two of the three bond angles between the phenol oxygen atom and the phosphate oxygen atoms (O_η–P–O_{nP}, where n = 1, 2, or 3) are smaller than 109.5°, the

Table 3. Selected bond angles and torsion angles of the phosphate group of the phosphotyrosine (degrees).

	CD28 [a]	Small molecule crystallography [b]		REFMAC [c]
		A	B	
Bond angles				
C_ζ–O_η–P	129.6	125.5	122.8	120.0
O_η–P–O_{1P}	94.7	103.2	108.3	108.2
O_η–P–O_{2P}	106.4	104.5	106.8	108.2
O_η–P–O_{3P}	110.8	106.9	103.7	108.2
(Average of O_η–P–O_{nP})	(104.0)	(104.9)	(106.3)	(108.2)
O_{1P}–P–O_{2P}	112.9	106.5	111.0	119.9
O_{2P}–P–O_{3P}	115.6	121.5	111.4	119.9
O_{3P}–P–O_{1P}	114.1	112.5	115.0	119.9
Torsion angles				
C_ζ–O_η–P–O_{1P}	−149.0	−85.4	61.2	–
C_ζ–O_η–P–O_{2P}	−33.4	25.7	178.8	–
C_ζ–O_η–P–O_{3P}	93.0	155.6	−58.5	–
(Rotation $O_{1P} \rightarrow O_{2P}$)	(115.6)	(111.1)	(117.6)	(120.0)
(Rotation $O_{2P} \rightarrow O_{3P}$)	(126.4)	(129.9)	(122.7)	(120.0)
(Rotation $O_{3P} \rightarrow O_{1P}$)	(118.0)	(119.0)	(119.7)	(120.0)

[a]Present work.
[b]Results from small-molecule X-ray crystallography [21]. As the asymmetric unit contains 2 phosphotyrosine molecules, denoted A and B, the values for both are shown.
[c]Values from the dictionary files of REFMAC.
doi:10.1371/journal.pone.0074482.t003

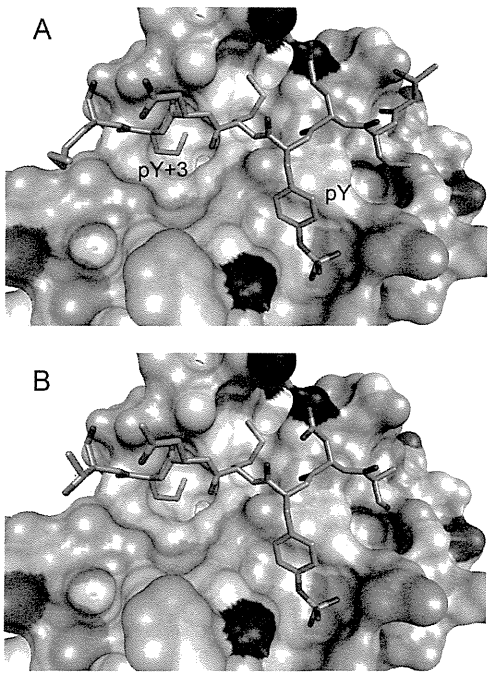

Figure 5. A model structure of the CD28-derived peptide bound to PI3K N. (A) The crystal structure of the amino-terminal SH2 domain of PI3K (PI3K N SH2) with a phosphopeptide derived from c-Kit (T-N-E-pY-M-D-M-K) and (B) a molecular model of PI3K N SH2 with the CD28-derived peptide (S-D-pY-M-N-M-T). The SH2 domains are shown as surface models, whereas the phosphopeptides are shown as stick models.
doi:10.1371/journal.pone.0074482.g005

theoretical value for ideal tetrahedral geometry, indicating that the phosphate oxygen atoms are somewhat more "spread up" than typical tetrahedral geometry. In addition, the 3 phosphate oxygens are in an asymmetrical arrangement, deviating from an equilateral triangle. To match one phosphate oxygen atom to another in a symmetrical arrangement, the rotation angle around the phenol oxygen-phosphorus bond (O_η–P) should be 120°. However, that is not the case for the phosphotyrosine in our structure. The difference between the maximum and minimum rotation angles is greater than 10°. Similar asymmetry is also observed in the phosphotyrosine molecule structures reported by small-molecule X-ray crystallography, whose resolution is 0.77 Å [21].

Discussion

Here, we reported the crystal structure of the Grb2 SH2 domain in complex with a phosphorylated peptide derived from CD28. The structure was determined at a resolution of 1.35 Å, the highest among the Grb2 SH2 domain structures reported to date. The structure revealed a unique feature of Grb2-SH2 binding to the CD28-derived peptide. In all previously reported Grb2 SH2/peptide complex structures, the peptide containing the phosphotyrosine residue adopted a type-I β-turn (Fig 2B) [19], except for the AICD-derived peptides in 2 Grb2 SH2/AICD structures [20]. The AICD-derived peptides have a proline residue at the pY+3 position and are incapable of forming a β-turn because proline does not have the amide hydrogen required for the characteristic hydrogen bond (Fig. 2C). The CD28-derived peptide reported here has a methionine residue at the pY+3 position, which is capable of forming the hydrogen bond. However, its structure is not a canonical type-I β-turn. Although it has a U-shaped conformation, similar to the β-turn, it is somewhat twisted and lacks the key hydrogen bond. This is the first such example.

The ψ angle of the asparagine at the pY+2 position seems to be largely responsible for this deviation from the type-I β-turn (Table 2). The larger value of the ψ angle moves the pY+3 residue slightly away from Grb2 SH2, making room for the side-chain of Met193^{pep}. In another words, this bulky side-chain lifted the peptide away from Grb2 SH2. The Grb2 SH2/peptide complex structures reported thus far have relatively small residues at the pY+3 position. Loss of the hydrogen bond may be compensated by the hydrophobic interaction between the methionine of the peptide and Grb2 SH2.

The φ angle of Met192^{pep} at the pY+1 position in our structure also deviates from that of the other Grb2 SH-bound peptides with type-I β-turns although the difference is smaller than that of the ψ angle discussed above. These 2 angles are complementary for maintaining the hallmark hydrogen bond, and the change in the φ angle of Met192^{pep} compensates for deviation of the ψ angle of Asn193^{pep} to some extent, keeping the 2 the main-chain oxygens of pTyr191^{pep} relatively close to the main-chain nitrogen of Met194^{pep}. The peptide may transiently adopt a type-I β-turn conformation in solution before binding to Grb2 SH2.

It is tempting to speculate that other peptides containing a residue with a large side chain may also adopt the twisted U-shape conformation, rather than the canonical type-I β-turn. Interestingly, when an epidermal growth factor (EGF)-derived peptide, which has a relatively large glutamine residue at the pY+3 position, is bound to Grb2 SH2 (PDB ID: 1ZFP), it adopts a conformation between the type-I β-turn and the twisted U-shape found in our structure [22]; both its ψ angle value (19.8°) and the O–N distance (3.37 Å) are intermediate between those of the type I β-turn and the twisted U-shape (Table 2).

In this study, the CD28-derived phosphopeptide binds to Grb2 SH2 in the twisted U-shape conformation. This phosphopeptide also binds to the SH2 domains of phosphatidylinositol 3-kinase (PI3K), whose consensus binding motif is pY-X-X-M. The crystal structure of the amino-terminal SH2 domain of PI3K (PI3K N SH2) containing a phosphopeptide derived from c-Kit [23] offers good insight into the interaction between the CD28-derived peptide and PI3K SH2 (Fig. 5A). The sequence of the c-Kit-derived peptide is TNE(pY)MDMKPGV, and this peptide bound to the SH2 domain in an extended conformation. A molecular model of the CD28-derived peptide bound to PI3K N SH2 can be made by simply replacing the sequence of the c-Kit peptide with that of the CD28-derived peptide, SD(pY)MNMT. The model would preserve most of the key protein-peptide interactions from the pY to pY+3 potions, with no obvious unfavorable interactions (Fig 5B). Therefore, one can expect that the CD28-derived peptide changes conformation in a receptor-dependent manner. The β-turn (or twisted U-shape) conformation of the Grb2 SH2-bound peptide positions the pY+2 residue close to the protein, making this residue highly conserved, whereas the extended conformation of the PI3K N SH2-bound peptide exposes the pY+2 residue to solvent, and it has no strong interactions with the protein. Instead, the residues in the pY+1 and pY+3 positions strongly interact with the protein. CD28 exploits the differences between the molecular recognition of pY by the PIK3 and Grb2 SH2 domains to enable binding to both proteins via a single pY site.

Acknowledgments

We thank Dr. Kentaro Tomii for helpful discussions. We also thank the technical staff at the Photon Factory, High Energy Accelerator Research Organization for maintenance of the beamline.

Author Contributions

Conceived and designed the experiments: NI RA MO. Performed the experiments: KH TI JT NI. Analyzed the data: NI HM. Contributed reagents/materials/analysis tools: HM. Wrote the paper: NI KH MO.

References

1. Lowenstein EJ, Daly RJ, Batzer AG, Li W, Margolis B, Lammers R, et al. (1992) The SH2 and SH3 domain-containing protein GRB2 links receptor tyrosine kinases to ras signaling. Cell 70: 431–442.
2. Rozakis-Adcock M, McGlade J, Mbamalu G, Pelicci G, Daly R, et al. (1992) Association of the Shc and Grb2/Sem5 SH2-containing proteins is implicated in activation of the Ras pathway by tyrosine kinases. Nature 360: 689–692.
3. McNemar C, Snow ME, Windsor WT, Prongay A, Mui P, et al. (1997) Thermodynamic and structural analysis of phosphotyrosine polypeptide binding to Grb2-SH2. Biochemistry 36: 10006–10014.
4. Ogura K, Tsuchiya S, Terasawa H, Yuzawa S, Hatanaka H, et al. (1999) Solution structure of the SH2 domain of Grb2 complexed with the Shc-derived phosphotyrosine-containing peptide. J Mol Biol 289: 439–445.
5. Rahuel J, Gay B, Erdmann D, Strauss A, Garcia-Echeverria C, et al. (1996) Structural basis for specificity of Grb2-SH2 revealed by a novel ligand binding mode. Nat Struct Biol 3: 586–589.
6. Thornton KH, Mueller WT, McConnell P, Zhu G, Saltiel AR, et al. (1996) Nuclear magnetic resonance solution structure of the growth factor receptor-bound protein 2 Src homology 2 domain. Biochemistry 35: 11852–11864.
7. Nioche P, Liu WQ, Broutin I, Charbonnier F, Latreille MT, et al. (2002) Crystal structures of the SH2 domain of Grb2: highlight on the binding of a new high-affinity inhibitor. J Mol Biol 315: 1167–1177.
8. Mueller DL, Jenkins MK, Schwartz RH (1989) Clonal expansion versus functional clonal inactivation: a costimulatory signalling pathway determines the outcome of T cell antigen receptor occupancy. Annu Rev Immunol 7: 445–480.
9. Schneider H, Cai YC, Prasad KV, Shoelson SE, Rudd CE (1995) T cell antigen CD28 binds to the GRB-2/SOS complex, regulators of p21ras. Eur J Immunol 25: 1044–1050.
10. Rudd CE, Schneider H (2003) Unifying concepts in CD28, ICOS and CTLA4 co-receptor signalling. Nat Rev Immunol 3: 544–556.
11. Rudolph R, Lilie H (1996) In vitro folding of inclusion body proteins. FASEB J 10: 49–56.
12. Winn MD, Ballard CC, Cowtan KD, Dodson EJ, Emsley P, et al. (2011) Overview of the CCP4 suite and current developments. Acta Crystallogr D Biol Crystallogr 67: 235–242.
13. McCoy AJ, Grosse-Kunstleve RW, Adams PD, Winn MD, Storoni LC, et al. (2007) Phaser crystallographic software. J Appl Crystallogr 40: 658–674.
14. Benfield AP, Teresk MG, Plake HR, DeLorbe JE, Millspaugh LE, et al. (2006) Ligand preorganization may be accompanied by entropic penalties in protein-ligand interactions. Angew Chem Int Ed Engl 118: 6984–6989.
15. Murshudov GN, Skubak P, Lebedev AA, Pannu NS, Steiner RA, et al. (2011) REFMAC5 for the refinement of macromolecular crystal structures. Acta Crystallogr D Biol Crystallogr 67: 355–367.
16. Emsley P, Lohkamp B, Scott WG, Cowtan K (2010) Features and development of Coot. Acta Crystallogr D Biol Crystallogr 66: 486–501.
17. Kraulis PJ (1991) MOLSCRIPT: a program to produce both detailed and schematic plots of protein structures. J Appl Crystallogr 24: 946–950.
18. DeLorbe JE, Clements JH, Whiddon BB, Martin SF (2010) Thermodynamic and structural effects of macrocyclic constraints in protein-ligand interactions. ACS Med Chem Lett 1: 448–452.
19. Ettmayer P, France D, Gounarides J, Jarosinski M, Martin MS, et al. (1999) Structural and conformational requirements for high-affinity binding to the SH2 domain of Grb2. J Med Chem 42: 971–980.
20. Das S, Raychaudhuri M, Sen U, Mukhopadhyay D (2011) Functional implications of the conformational switch in AICD peptide upon binding to Grb2-SH2 domain. J Mol Biol 414: 217–230.
21. Suga M, Inubushi C, Okabe N (1998) *O*-Phospo-L-tyrosine. Acta Cryst C54: 83–85.
22. Rahuel J, Garcia-Echeverria C, Furet P, Strauss A, Caravatti G, et al. (1998) Structural basis for the high affinity of amino-aromatic SH2 phosphopeptide ligands. J Mol Biol 279: 1013–1022.
23. Nolte RT, Eck MJ, Schlessinger J, Shoelson SE, Harrison SC (1996) Crystal structure of the PI3-kinase p85 amino-terminal SH2 domain and its phosphopeptide complexes. Nat Struct Biol 3: 364–374.

Jpn. J. Infect. Dis., 66, 375-378, 2013

Original Article

Changing Burden of HIV/AIDS to Clinical Settings in Northern Thailand over 15 Years

Panita Pathipvanich[1†], Naho Tsuchiya[2,3†], Archawin Rojanawiwat[4], Wolf-Peter Schmidt[2,5], Wattana Auwanit[4], Pathom Sawanpanyalert[4], and Koya Ariyoshi[2,3*]

[1]*Day Care Center, Lampang Hospital, Lampang;*
[4]*National Institute of Health, Department of Medical Sciences, Ministry of Public Health, Nonthaburi, Thailand;*
[2]*Department of Clinical Medicine, Institute of Tropical Medicine and*
[3]*Global COE Programme, Nagasaki University, Nagasaki, Japan; and*
[5]*Environmental Health Group, Disease Control & Vector Biology Unit, London School of Hygiene and Tropical Medicine, London, UK*

(Received July 30, 2012. Accepted May 7, 2013)

SUMMARY: We conducted a hospital-based descriptive study to describe the changing pattern of patient numbers, characteristics, and mortality rates among human immunodeficiency virus (HIV)-infected patients in northern Thailand over 15 years. The survival status on October 31, 2010 of all HIV-infected adults who attended an HIV center in a government hospital between 1995 and 2010 was ascertained. In total, 3,706 patients were registered, 2,118 (57.2%) of which were male. The survival status of 3,439 patients (92.9%) was available. In addition, 1,543 deaths were identified out of 12,858 person-year-observations (PYO) resulting in a mortality rate of 12.4 deaths/100 PYO (95% confidence interval [CI], 11.3–13.0). An initial decline in mortality rates was observed prior to 1999, probably because of an increase in the proportion of less symptomatic patients. After the introduction of the national highly active antiretroviral therapy (HAART) program, a profound decline in mortality rates was observed, reaching 2.0 deaths/100 PYO (95% CI, 1.4–2.9) in 2010. Simultaneously, the number of patients on follow-up increased by nearly fourfold. Although HAART has drastically improved the survival of HIV-infected patients, the number of patients receiving therapy at this HIV clinic has substantially increased. While referral of HIV patients to general physicians' care should be urged, we cannot overemphasize the importance of preventing new HIV infections.

INTRODUCTION

Thailand has been one of the first Asian countries to be severely affected by the human immunodeficiency virus (HIV) epidemic. Initially, HIV mainly spread between female sex workers and their male clients. These males subsequently transmitted HIV to their wives, who passed it on to their newborn babies (1). The situation was particularly severe in northern Thailand, including Lampang province. Since 1985, when the HIV epidemic began, Lampang province has had the 5th highest prevalence of HIV in Thailand (2). Since the mid-1990s, HIV prevalence in adults has declined from an estimated peak of 2.1% to 1.4% in 2007 (3).

Our first survival survey on HIV-infected patients attending Lampang Hospital completed in October 1999 and suggested a mortality rate of approximately 50/100 person-year-observations (PYO) among patients (4). A number of government initiatives have substantially impacted HIV care in Thailand. The Prevention of Mother-to-Child Transmission (PMTCT) program began in northern Thailand in 1997 (5). As part of this program, the Thai government health services began to screen all pregnant women, allowing the early detection of HIV infections and provision of short-course zidovudine prophylaxis to prevent vertical transmission. Furthermore, the government enhanced the promotion of education on HIV and the development of care and support for HIV-infected patients. In 2003, the National Access to Antiretroviral Program for People Living with HIV/AIDS (NAPHA) was launched (6). This improved patient access to highly active antiretroviral therapy (HAART), particularly by the use of a fixed-dose combination of generic drugs (GPOvir®: stavudine, lamivudine, and nevirapine). By December 2007, the estimated antiretroviral drug coverage in Thailand had reached 61% (47–81%) (2).

In this study, we describe the changing pattern of patient numbers, characteristics, and mortality rates among HIV-infected patients in northern Thailand and accordingly discuss the effect of the introduction of NAPHA and other government programs on HIV care in northern Thailand.

MATERIALS AND METHODS

We present data from a hospital-based descriptive study conducted in a large hospital in northern Thailand. Lampang Hospital is the only government

*Corresponding author: Mailing address: Department of Clinical Medicine, Institute of Tropical Medicine, Nagasaki University, 1-12-4 Sakamoto, Nagasaki City 852-8523, Japan. Tel: +81-95-819-7842, Fax: +81-95-819-7843, E-mail: kari@nagasaki-u.ac.jp
†These two authors contributed equally to this work.

referral hospital with approximately 800 beds in Lampang province, located 100 km south of the city of Chiang Mai. In October 1995, an HIV center, locally called a day care center, was established at this hospital to provide comprehensive care to HIV-infected patients, including psychosocial care and support for patient self-help groups. This center functioned as a referral outpatient clinic and provided medical care to by far the largest number of HIV patients in the province. All HIV-infected patients registered at the center from October 2, 1995 to October 31, 2010 were included in the present study. Demographic and clinical information at the time of registration was obtained from medical charts and hospital records. For this analysis, we ascertained the survival status of all HIV-infected patients over 16 years of age who attended the HIV clinic in Lampang Hospital during that time using hospital records, death certificates from the Lampang Provincial Health Office, and postal letters as well as by contacting their families or relatives. Patients known to be attending other hospitals within Lampang province and having no death certification by the Lampang Provincial Health Office were regarded as being alive. If the exact date was unknown, the death was assumed to have occurred on the 15th of a month (if the day of the month was missing) and in June (if information on the month was missing). Loss of follow-up was defined as patients no longer residing within Lampang province, those whose survival status was unknown, or those who died but the year of death was not available. We calculated the number of patients and mortality rate over the period of October 2, 1995 to October 31, 2010. We present changes in crude survival rates at 12-month intervals over the study period in patients attending the center during each 12-month period. The number of patients who began HAART was shown to investigate the impact of HAART on the change in mortality rates.

This study was conducted as part of the Lampang HIV-Cohort Phase I and Lampang and Phayao HIV Cohort Phase II studies, which were approved by Thai Ministry of Public Health Ethics Committee.

RESULTS

Between 1995 and 2010, a total of 3,706 patients received care at the day care center. Of these, 2,118 (57.2%) were male, and the median age was 33.8 years (interquartile range [IQR], 33.5–34.1; range, 15–84). Approximately 95% of transmission routes were attributed to heterosexual intercourse (4,7,13). There was no significant change in the median age over time. Baseline CD4 cell counts were obtained from 3,111 patients (83.9%). The median CD4 cell count was 81 (IQR, 22–262). Figure 1A shows the number of newly registered patients at the HIV clinic for each 12-month study period. At the beginning of the study period, the number of the newly registered male patients was twofold greater than that of female patients. The gap gradually decreased as more women who were infected by their partners attended the HIV clinic. A temporal increase was observed from 2000 to 2003, possibly due to the effect of our prospective cohort that began in July 2000 and the initiation of NAPHA. Thereafter, the number of newly registered patients has gradually declined. Figure 1B shows the proportion of patients stratified by a CD4 cell count of <50 cells/μl, 50–200 cells/μl, and >200 cells/μl at the first visit. The proportion of patients with a CD4 cell count >200 cells/μl temporally increased around 2,000 (38.1%) and then stabilized since 2008, reaching 40% in 2010.

The survival status on October 31, 2010 was available for 3,439 patients (92.9%). In total, 267 patients were lost to follow-up. The median follow-up duration was 1,689 days (IQR, 799–2,680; range, 0–4,318). A total of 1,543 deaths were identified out of 12,858 PYO, resulting in an overall mortality rate of 12.4 deaths/100 PYO (95% confidence interval [CI], 11.3–13.0). Figure 1C shows temporal changes in the mortality rate in the total population, stratified by gender, at 12-month intervals. Mortality rates declined from 54/100 PYO (95% CI, 47–63) in 1998 to 33/100 PYO (95% CI, 28–40) in 1999, remaining around this level until about 2002. HAART was first conducted among a restricted number of patients around 2000 as a pilot phase and has been broadly provided by NAPHA since 2003. Consequently, the number of patients on HAART has been continuously increasing (Fig. 1D). Following the introduction of NAPHA, a further pronounced decline in mortality rates was observed from 2003, reaching as low as 2.0 deaths/100 PYO in 2010 (95% CI, 1.4–2.9). The mortality rate of males was higher than that of females, particularly before the HAART era. A decline in mortality rates prior to the introduction of HAART was greater in males than in females. Figure 1E shows the proportion of patients who died within 3 months after the first visit, stratified by gender. Before 2005, male patients were more likely to die early than female patients. Interestingly, there was a sharp increase in this trend after 2008. The cumulative number of patients on active follow-up remained stable before 2001 (Fig. 1F). From 2001 to 2010, particularly after NAPHA was initiated in 2003, the number of patients being actively followed-up drastically increased by nearly fourfold.

DISCUSSION

In the present study, we described changes in mortality rates among HIV-infected patients and the healthcare burden, such as numbers and characteristics of patients, over 15 years in northern Thailand. Although we demonstrated that the mortality rate declined with an increase in the number of patients on HAART (Fig. 1C and 1D), it may not be explained by the direct effect of HAART alone. Particularly, the initial decline in mortality well before the launch of NAPHA, was thought to be due to an increased proportion of less symptomatic patients. During the early phase of the HIV epidemic, before the Thai government launched various programs against social stigmatization of HIV/AIDS (6), patients often did not seek care until they were critically ill. We believe that unfavorable treatment-seeking behavior related to the social stigma of HIV/AIDS contributed to the very high mortality rate prior to 1999. The extended national PMTCT program, promotion of education on HIV, and development of care and support for HIV-infected patients have also played a role in the increase in the number of less symptomatic patients attending the HIV clinic. Apart from its effect on viral load, the mere

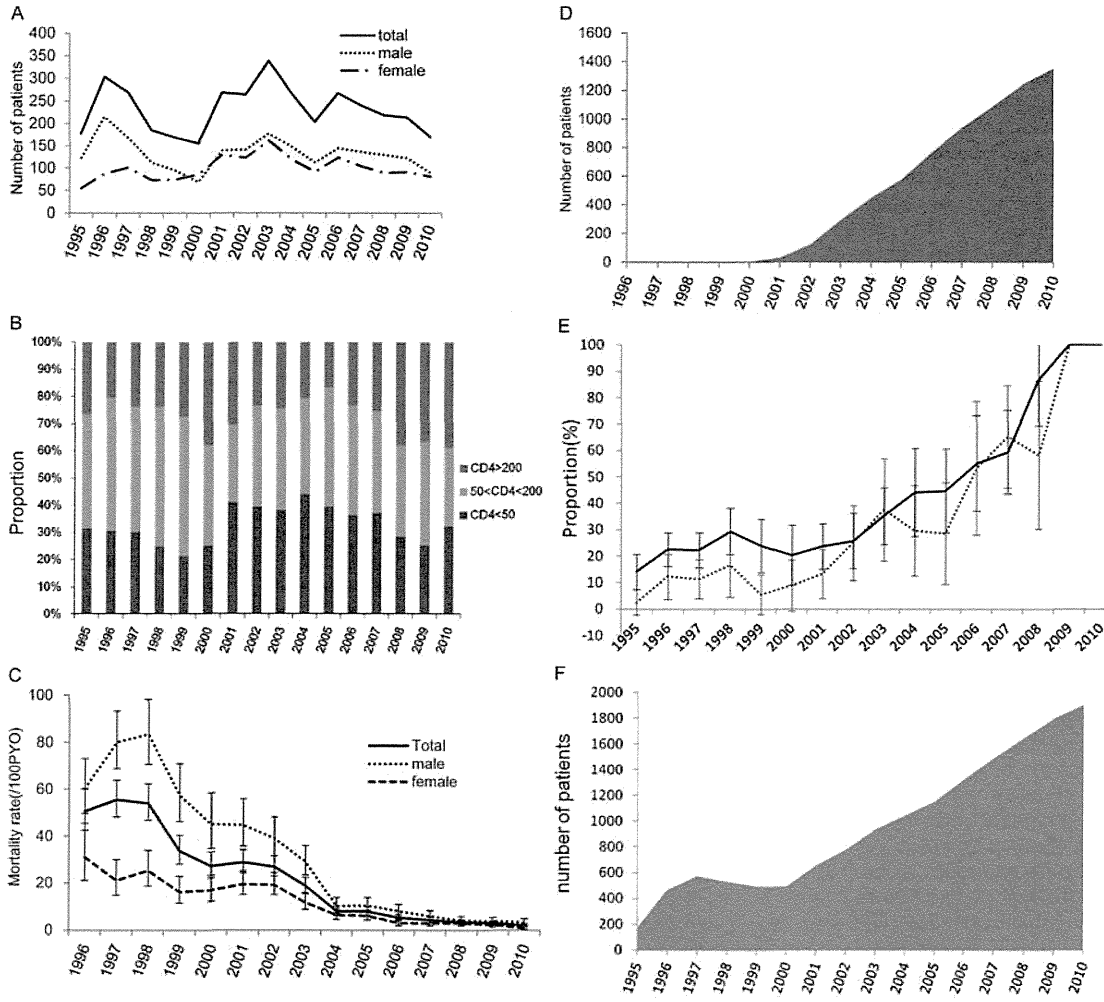

Fig. 1. (A) Number of newly registered patients. (B) Proportion of patients stratified by a CD4 cell count at enrolment. (C) Mortality rate with 95% confidence interval. (D) Number of patients on highly active antiretroviral therapy. (E) Proportion of deaths which occurred within the first 3 months of registration; denominator is the number of total death each year. (F) Cumulative number of patients on active follow-up. The pilot phase of access to antiretroviral therapy program started in 2000. The National Access to Antiretroviral Program for People Living with HIV/AIDS (NAPHA) was launched universally in 2003.

availability of HAART may have improved survival after 2003 by encouraging HIV-infected patients to seek support from healthcare and possibly from social services. Our previous qualitative study showed that the availability of HAART had a positive impact on the attitudes and self-confidence of HIV-infected patients, including a markedly lower perceived sense of stigmatization (7). The availability of treatment also changed the practice of healthcare professionals; their morale was boosted and awareness toward the diagnosis of opportunistic infections was heightened because death from AIDS-related infections is no longer perceived as unavoidable.

Despite the many positive effects of improving access to HAART, we identified a number of issues of concern. First, the local healthcare staff perceive that the long-term side effects of antiretroviral drugs are becoming a major problem (8). It has been shown that among the active substances in GPOvir®, only stavudine is known to frequently cause lipodystrophy (9,10). The longer patients are on antiretroviral therapy, the higher the risk of long-term side effects or metabolic changes (11), resulting in regimen modification. Given that the choice of salvage regimen is still limited in low- and middle-income countries, further studies investigating the long-term outcomes of HAART and its predictors are warranted.

Second, the incidence of early death (within 3 months after recruitment) (Fig. 1E) drastically increased during the HAART era, reflecting that while the total number of deaths decreased, most involved cases who had advanced AIDS prior to their first visit and died soon after the recruitment period. Although the cause of death is generally difficult to obtain in a busy government hospital, our previously published studies with active investigations indicated that most deaths were attributed

to HIV-related illnesses that occurred during both the pre- and post-HAART era (7,12,14). Our previous study revealed the highest incidence of opportunistic infections during the first year of HAART, particularly among patients with a low CD4 cell count (13). Some patients died before initiating HAART. Even during the HAART era, special attention should be paid to the management of newly registered patients, and we should continue to make an effort to reduce the number of undiagnosed HIV-infected patients.

Third, this study demonstrated that the rapid increase in the number of outpatients in this setting shortly after NAPHA was a result of the increase in the number of patients on HAART and decrease in the mortality rate. The HIV clinic is now faced with a large number of patients, which has resulted in a higher workload for the staff. At the same time, the number of inpatients with opportunistic infections has considerably declined. Since the initiation of NAPHA, the AIDS ward of Lampang Hospital became redundant and closed in January 2004. Overall, it remains unclear whether the overall workload due to HIV has increased or decreased following the introduction of HAART. However, the burden of care at this HIV clinic will continue to increase unless the actual number of newly infected patients substantially decreases. While we cannot overemphasize the importance of preventing new HIV infections, referral of HIV-patients to general physicians' care once their first-line therapy is stabilized should be urged; however, this will require additional training resources to build on the success of the ongoing programs for ensuring adequate care for HIV-infected patients in Thailand.

Acknowledgments This study was supported by Japan International Co-operation Agency (JICA), Japan Health Science Foundation, and the Department of Medical Sciences of Ministry of Public Health of Thailand and partially by Global COE Programme, Nagasaki University.

We would like to thank all the patients and staff at Lampang Hospital especially Ms. S Kasemsuk, Ms. S Seneewong-Naayudhaya, Ms. A Suyasarojna, Mr. P Wongnamnong, and Ms. K Yoddumnern, Ms. K Lor-yont, Mr. W Khaewkarnka, Mr. S Umnajsirisuk, and Mr. S Niyom-thai.

Conflict of interest None to declare.

REFERENCES

1. Ruxrungtham, K., Brown, T. and Phanuphak, P. (2004): HIV/AIDS in Asia. Lancet, 364, 69–82.
2. Ministry of Public Health, Thailand (2008): Epidemiological Information Section Bureau of Epidemiology, Department of Disease Control, Ministry of Public Health, Thailand.
3. Joint United Nations Programme on HIV/AIDS (UNAIDS)/World Health Organization (WHO) (2010): Epidemiological Fact Sheets on HIV and AIDS, Thailand, Update.
4. Pathipvanich, P., Ariyoshi, K., Rojanawiwat, A., et al. (2003): Survival benefit from non-highly active antiretroviral therapy in a resource-constrained setting. J. Acquired Immune Defic. Syndr., 32, 157–160.
5. Kanshana, S. and Simonds, R.J. (2002): National program for preventing mother-child HIV transmission in Thailand: successful implementation and lessons learned. AIDS, 16, 953–959.
6. World Health Organization (WHO) (2005): External Review of the Health Sector Response to HIV/AIDS in Thailand. Ministry of Public Health, Thailand and WHO Regional Office for South-East Asia.
7. Tsuchiya, N., Pathipvanich, P., Yasuda, T., et al. (2009): Demographic, socio-economic, behavioral and clinical factors predicting virologic failure with generic fixed-dose combination antiretroviral therapy before universal health insurance coverage in northern Thailand. Southeast Asian J. Trop. Med. Public Health, 40, 71–82.
8. Tsuchiya, N., Pathipvanich, P., Rojanawiwat, A., et al. (2012): HLA-B*3505 and female gender were strong predictive factors of modifying the first ARV drug regimen due to adverse effect: Thailand. 19th Conference on Retroviruses and Opportunistic Infections, March 5–8, 2012, Seattle, WA, USA.
9. van Griensven, J., De Naeyer, L., Mushi, T., et al. (2007): High prevalence of lipoatrophy among patients on stavudine-containing first-line antiretroviral therapy regimens in Rwanda. Tran. R. Soc. Trop. Med. Hyg., 101, 793–798.
10. Subbaraman, R., Chaguturu, S.K., Mayer, K.H., et al. (2007): Adverse effects of highly active antiretroviral therapy in developing countries. Clin. Infect. Dis., 45, 1093–1101.
11. Carr, A. and Cooper, D.A. (2000): Adverse effects of antiretroviral therapy. Lancet, 356, 1423–1430.
12. Pathipvanich, P., Rojanawiwat, A., Ariyoshi, K., et al. (2004): Mortality analysis of HIV-1 infected patients for prioritizing antiretroviral drug therapy. J. Med. Assoc. Thai, 87, 951–954.
13. Rojanawiwat, A., Tsuchiya, N., Pathipvanich, P., et al. (2011): The impact of the National Access to Antiretroviral Program on the incidence of opportunistic infections in Thailand. Int. Health, 3, 101–107.
14. Tsuchiya, N., Pathipvanich, P., Rojanawiwat, A., et al. (2012): Chronic hepatitis B and C co-infection increased all cause mortality among HAART naïve HIV patients in northern Thailand. Epidemiol. Infect., Nov 1:1–9 [Epub ahead of print]. doi:10.1017/S0950268812002397.

Infection of Adult Thymus with Murine Retrovirus Induces Virus-Specific Central Tolerance That Prevents Functional Memory CD8$^+$ T Cell Differentiation

Shiki Takamura[1]*, Eiji Kajiwara[1], Sachiyo Tsuji-Kawahara[1], Tomoko Masumoto[1], Makoto Fujisawa[1], Maiko Kato[1], Tomomi Chikaishi[1], Yuri Kawasaki[1], Saori Kinoshita[1], Manami Itoi[2], Nobuo Sakaguchi[3], Masaaki Miyazawa[1]*

1 Department of Immunology, Kinki University Faculty of Medicine, Osaka, Japan, **2** Department of Immunology and Microbiology, Meiji University of Integrative Medicine, Kyoto, Japan, **3** Department of Immunology, Kumamoto University School of Medicine, Kumamoto, Japan

Abstract

In chronic viral infections, persistent antigen presentation causes progressive exhaustion of virus-specific CD8$^+$ T cells. It has become clear, however, that virus-specific naïve CD8$^+$ T cells newly generated from the thymus can be primed with persisting antigens. In the setting of low antigen density and resolved inflammation, newly primed CD8$^+$ T cells are preferentially recruited into the functional memory pool. Thus, continual recruitment of naïve CD8$^+$ T cells from the thymus is important for preserving the population of functional memory CD8$^+$ T cells in chronically infected animals. Friend virus (FV) is the pathogenic murine retrovirus that establishes chronic infection in adult mice, which is bolstered by the profound exhaustion of virus-specific CD8$^+$ T cells induced during the early phase of infection. Here we show an additional evasion strategy in which FV disseminates efficiently into the thymus, ultimately leading to clonal deletion of thymocytes that are reactive to FV antigens. Owing to the resultant lack of virus-specific recent thymic emigrants, along with the above exhaustion of antigen-experienced peripheral CD8$^+$ T cells, mice chronically infected with FV fail to establish a functional virus-specific CD8$^+$ T cell pool, and are highly susceptible to challenge with tumor cells expressing FV-encoded antigen. However, FV-specific naïve CD8$^+$ T cells generated in uninfected mice can be primed and differentiate into functional memory CD8$^+$ T cells upon their transfer into chronically infected animals. These findings indicate that virus-induced central tolerance that develops during the chronic phase of infection accelerates the accumulation of dysfunctional memory CD8$^+$ T cells.

Citation: Takamura S, Kajiwara E, Tsuji-Kawahara S, Masumoto T, Fujisawa M, et al. (2014) Infection of Adult Thymus with Murine Retrovirus Induces Virus-Specific Central Tolerance That Prevents Functional Memory CD8$^+$ T Cell Differentiation. PLoS Pathog 10(3): e1003937. doi:10.1371/journal.ppat.1003937

Editor: Michael S. Diamond, Washington University School of Medicine, United States of America

Received July 18, 2013; **Accepted** January 7, 2014; **Published** March 20, 2014

Funding: This work was supported by grants-in-aid for scientific research from Ministry of Education, Culture, Sports, Science and Technology of Japan, including the High-Tech Research Center and Anti-Aging Center projects, those from the Japan Society for Promotion of Science, KAKENHI (B), those from the Ministry of Health, Labor and Welfare of Japan for Research on HIV/AIDS (MM), a Grant-in-Aid for Young Scientists (B), and grants from The Ichiro Kanehara Foundation, Astellas Foundation for Research on Metabolic Disorders (ST). The funders had no role in study design, data collection and analysis, decision to publish, or preparation of the manuscript.

Competing Interests: The authors have declared that no competing interests exist.

* E-mail: takamura@med.kindai.ac.jp (ST); masaaki@med.kindai.ac.jp (MM)

Introduction

Antigen-specific CD8$^+$ T cell populations are a major component that eliminate cells infected with intracellular pathogens. After infections that are cleared acutely, antigen-specific CD8$^+$ T cells can differentiate into functionally competent memory CD8$^+$ T cells, and can persist for a long time in the apparent absence of relevant antigens [1]. In contrast, in the case of chronic infections where the antigens are presented persistently, CD8$^+$ T cells primed during the early phase of infection succumb to progressive functional defects, such as impaired ability to proliferate, kill infected cells, and/or produce effector cytokines in response to the antigen-specific stimulation [2]. In most cases, this loss of effector functions is due to signaling through inhibitory molecules such as programmed cell death 1 (PD-1), lymphocyte activation gene 3 (LAG-3), CD244, CD160, and T cell Ig domain and mucin domain 3 (Tim-3), and is called exhaustion [2]. The severity of this dysfunction, which is in correlation with the numbers and extent of inhibitory molecules expressed on exhausted CD8$^+$ T cells, is critically linked with the levels of repetitive exposure to the relevant antigen [3]. In addition to their negative effects on the functionality of antigen-experienced CD8$^+$ T cells, persisting antigens also induce stable proliferation of already-exhausted memory CD8$^+$ T cells [4]. The resultantly sustained numbers of functionally impaired memory CD8$^+$ T cells potentially inhibit optimal priming of otherwise functional fresh memory CD8$^+$ T cells via physiological competition for the niche. Thus, chronic infection is a vicious circle of ongoing CD8$^+$ T cell dysfunction and ineffective antigen clearance. Despite such detrimental effects, however, recent studies shed light on a beneficial role of persistent antigens on the functionalities of memory CD8$^+$ T cells. Naïve CD8$^+$ T cells are continuously provided from the thymus even during the chronic phase of infection, and this continual thymic output can result in the priming of new antigen-specific CD8$^+$ T

Author Summary

During thymocyte development, cells that recognize self-antigens are specifically deleted by the process known as negative selection. However, some pathogens disseminate to the thymus, and can induce foreign antigen presentation within this organ, resulting in potentially harmful clonal deletion of pathogen-specific T-lymphocyte precursors. In chronic infections, pathogen-specific T cells in the periphery progressively lose their functionality due to continual stimulation with the persisting antigen, a phenomenon known as T cell exhaustion. However, pathogen-reactive naïve T cells freshly primed during the chronic phase of infection can nevertheless replenish the functional pool of memory T cells. Therefore, a lack of their generation in the face of peripheral exhaustion may ultimately cause the loss of functional memory T cells and the resultant lack of pathogen control. In this study, we demonstrate that Friend murine retrovirus can utilize the above immune evasion strategy, a combination of ongoing peripheral exhaustion and virus-induced central tolerance. Our data suggest that, along with the reinvigoration of exhausted T cells in the periphery, preservation of the thymic function in supplying pathogen-specific naïve T cells may be important when considering immunological control of chronic infection with thymotropic pathogens.

cells [5]. Unlike exhausted $CD8^+$ T cells that were primed in the early phase of infection, $CD8^+$ T cells primed during the chronic phase of infection in low-antigen and less intensive inflammatory settings give rise to functional memory $CD8^+$ T cells capable of mounting authentic recall responses [6]. Similar memory-dominated differentiation of $CD8^+$ T cells can also be found when $CD8^+$ T cells are primed after the peak of an acute infection, by the time that the majority of antigens have been cleared out [7]. Thus, persistent antigens play an important role in generating functional memory $CD8^+$ T cells in the presence of continual thymic output.

Friend virus (FV) is a murine retrovirus complex comprising two gammaretroviruses: replication-competent Friend murine leukemia virus (F-MuLV) and replication-defective spleen focus-forming virus (SFFV) [8]. Although FV particles can bind onto the surfaces of a wide variety of cells via cationic amino acid transporter as an entry receptor [9,10], viral replication occurs preferentially in actively dividing hematopoietic cells, especially in erythroid progenitor cells in the bone marrow (BM) and spleen [8]. In the susceptible strains of mice [e.g. (C57BL/6×A/WySnJ)F_1 ($B6AF_1$) mice], SFFV gp55 envelope glycoprotein stimulates erythropoietin receptor in conjunction with its binding to the short form of hematopoietic cell-specific receptor tyrosine kinase Stk/Ron, resulting in massive expansion of virus-infected erythroblasts [11,12]. As a result, FV-infected mice develop severe splenomegaly associated with polycythemia and high-level viremia [8]. This acute pathogenesis ultimately causes leukemia development in some cases, but most $B6AF_1$ mice recover from the above initial splenomegaly and survive. Following recovery, however, FV establishes a lifelong chronic infection and mice are never able to completely eradicate this virus [13]. Although antigen levels are low during the chronic phase of infection, it is sufficient to prime antigen-specific $CD8^+$ T cells, as adoptively transferred FV-specific $CD8^+$ T cells can be activated and acquire effector functions in chronically infected animals [14]. However, the precise effect of persistent antigens on the functionalities of FV-specific memory $CD8^+$ T cells remains unclear.

It has been proposed that FV-specific $CD8^+$ T cells progressively lose their effector functions during the chronic phase of infection due to suppression by virus-induced regulatory T cells (Tregs) [14–20]. In $B6AF_1$ mice, however, we found that severe dysfunction of FV-specific $CD8^+$ T cells appeared even during the acute phase of infection in the absence of an apparent increase in Treg functions, and this was critically related with the FV-induced acute pathogenesis [21]. At the peak of infection, numbers of virus-infected erythroblasts in the spleen reached more than 10^8, comprising approximately 75% of total splenocytes. These virus-infected erythroblasts intensively expressed programmed death ligand 1 (PD-L1) and MHC class I, thereby creating a highly tolerogenic environment. Consequently, FV-specific effector $CD8^+$ T cells suffered rapid exhaustion, and most of these cells were incapable of responding to restimulation with FV-encoded antigens [21]. Since effector $CD8^+$ T cells generated in the absence of the splenomegaly in mice inoculated with F-MuLV alone showed less exhausted phenotypes as compared to those generated in the presence of splenomegaly, SFFV-induced pathogenesis was shown to be mainly responsible for the severe and rapid exhaustion of antigen-specific effector $CD8^+$ T cells [21]. In the current study, we further extended our previous study, and found that functional memory $CD8^+$ T cells were rarely detected in FV-infected mice even during the chronic phase of infection. This severe dysfunction was apparently exclusive to FV-specific $CD8^+$ T cells but not found in FV-unrelated $CD8^+$ T cells. As a basis for this antigen-specific memory T cell dysfunction, FV is shown to disseminate to the thymus and induce virus-specific central tolerance, thereby preventing the generation of virus-specific naïve $CD8^+$ T cells. Thus, the severe dysfunction of FV-specific memory $CD8^+$ T cells is likely due to a combination of ongoing peripheral exhaustion and the deletion of virus-reactive thymocytes.

Results

FV disseminates to and persists in the thymus following infection

Infection of $B6AF_1$ mice with FV results in the expansion of virus-infected erythroblasts that causes severe exhaustion of antigen-specific $CD8^+$ T cells even during the acute phase of infection [21]. During the chronic phase of FV infection where the progressive expansion of virus-infected erythroblasts has resolved, FV-specific naïve $CD8^+$ T cells must be continuously provided from the thymus. If this is the case, newly recruited FV-specific naïve $CD8^+$ T cells should be primed with persistent FV antigens in the absence of expanded virus-infected erythroblasts. These newly primed $CD8^+$ T cells may then participate in the FV-specific $CD8^+$ T cell responses with better functionalities than the above exhausted cells [5]. However, most of the virus-specific memory $CD8^+$ T cells in the BM and spleen still retained highly exhausted phenotypes even more than 6 weeks after infection, as determined by the expression of multiple inhibitory receptors, PD-1, LAG-3, and Tim-3 on their surfaces (Figure S1A, B). Levels of expression of these inhibitory receptors were much higher on virus-specific $CD8^+$ T cells in the BM than on those in the spleen, indicating that during the chronic phase of infection, memory $CD8^+$ T cells received more abundant antigenic stimulation in the former tissue (Figure S1B). As most virus-specific $CD8^+$ T cells succumb to irreversible exhaustion even during the early phase of infection [21], the above phenotypically exhausted memory $CD8^+$ T cells in chronically infected mice were no longer reinvigorated by the administration of PD-1-blocking antibody (data not shown). In support of this, almost no FV antigen-reactive IFN-γ

production from $CD8^+$ T cells was detected when FV-infected mice were later challenged with FBL3 tumor cells, a potent inducer of FV-specific $CD8^+$ T cell responses, and the cells were restimulated with the MHC class I-restricted viral antigenic peptide (Figure S1C, D). These virus-infected mice also failed to control FBL3 tumor progression, similar to those that received syngenic tumor cells, EL-4, while uninfected mice rapidly rejected the tumor (Figure S1E, F). Based on these observations, we started to ask if FV infection influences the continuous recruitment of virus-specific naïve $CD8^+$ T cells from the thymus.

It has been reported that the BM and spleen are the major organs where massive replication of FV takes place [8]. Large numbers of virus-producing cells were already found in the BM at as early as 1 week post infection, and their numbers in the spleen reached a peak by 2 weeks post infection (Figure 1A). Despite a gradual decline after the peak of infection, significant numbers of virus-producing cells could still be detected until at least 10 weeks post infection, indicating that FV established persistent infection in these organs (Figure 1A). Surprisingly, significant numbers of virus-producing cells were also detected in the thymus at 2 weeks post infection, followed by the establishment of persistent infection in this organ (Figure 1A). At 2 weeks post FV infection, both F-MuLV and SFFV mRNA were detected from the thymus, but the levels of SFFV mRNA expression were much lower than those of F-MuLV mRNA in this organ (Figure 1B). Using the monoclonal antibody specific for F-MuLV envelope glycoprotein gp70 we found that it is mainly double positive (DP) and double negative (DN) thymocytes that harbor F-MuLV in the thymus, as up to 50% of cells in these populations were expressing gp70 on their surfaces at the peak of infection (Figure 2A and Figure 3A). Surface expression of F-MuLV gag p15 antigen was also detected on gp70-expressing DN and DP thymocytes (Figure 3B), indicating the presence of glycosylated gag protein ($gPr75^{gag}$). Further, when thymocytes were fixed and permeabilized, F-MuLV capsid p30 antigen was also detected in $gp70^+$ DN and DP thymocytes (data not shown). These results indicate that F-MuLV gene products were actively synthesized in DN and DP thymocytes. Immunohistochemical analyses also revealed viral gag antigen expression throughout the cortex where the DN and DP thymocytes were distributed (Figure 3C). Interestingly, the spread of the virus into the thymus appeared to be delayed a week as compared to that in the BM and spleen (Figure 1), suggesting that the dissemination of the virus to the thymus occurred following massive viral replication in the BM and spleen. In support of this, only marginal increases in proportions of $gp70^+$ cells in the thymus were observed when *Fv2*^{r} C57BL/6 (B6) mice lacking the expression of the short form of STK (sf-Stk) were infected with FV or $B6AF_1$ mice were inoculated with F-MuLV alone (Figure S2). Thus SFFV-induced proliferation of FV-infected erythroid cells is required for effective dissemination of FV into the thymus.

Notably, $CD44^{hi}$ DN thymocytes virtually lacked the expression of gp70, indicating that T cell progenitors migrated from the BM were not an initial source of virus dissemination to the thymus (Figure 2A). Since FV proviruses are known to be preferentially integrated into proliferating cells, and a large proportion of $CD44^-$ DN thymocytes were $gp70^+$, it is likely that FV initially infects DN thymocytes within this organ, and then replicates vigorously in DN thymocytes that proliferate and differentiate into DP thymocytes. The highest number of virus-producing cells in

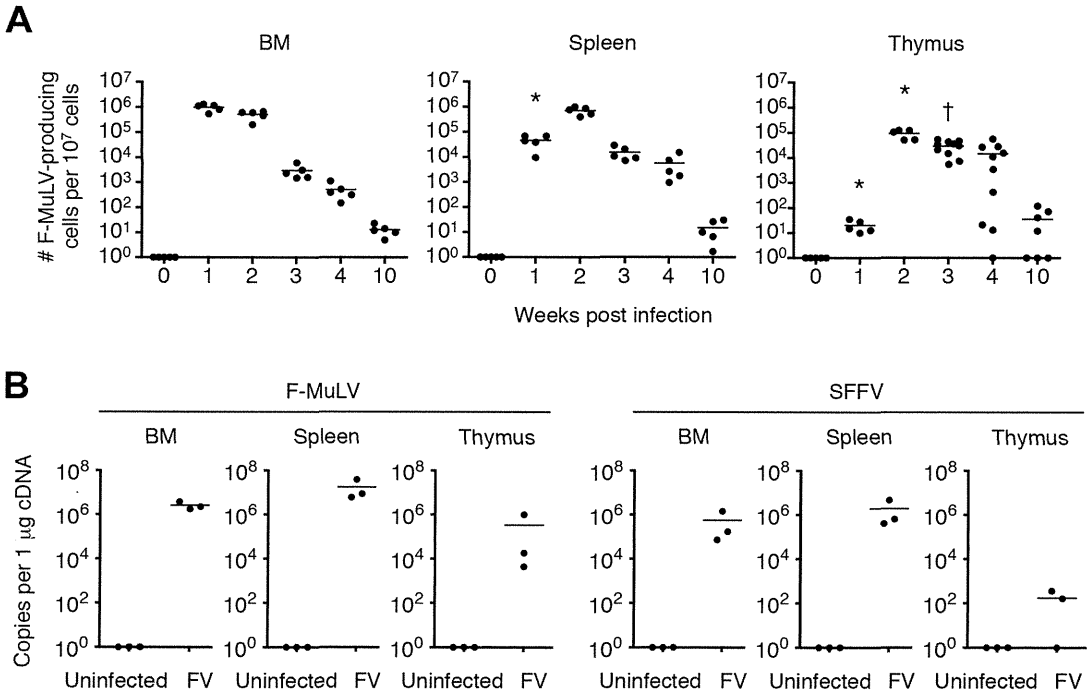

Figure 1. FV disseminates to and persists in the thymus following infection. Mice were infected with 1,000 SFFU of FV. (A) Cells in the BM, spleen and thymus were isolated at indicated time-points, and were cocultured with *M. dunni* cells to enumerate F-MuLV infectious centers. Each symbol represents an individual mouse. Data are representative of two independent experiments with essentially equivalent results. *, $p<0.0001$ in comparison with the numbers of FV-producing cells in the BM at the same time-point; †, $p<0.0001$ in comparison with those in the spleen, by two-way ANOVA with Bonferroni's correction for multiple comparisons. (B) Total RNA was purified from the BM, spleen and thymus of FV-infected mice at day 14. Expression levels of F-MuLV and SFFV mRNA were analyzed by quantitative real-time PCR assays. Shown are copy numbers of viral DNA fragments amplified from 1 μg of total cDNA.
doi:10.1371/journal.ppat.1003937.g001

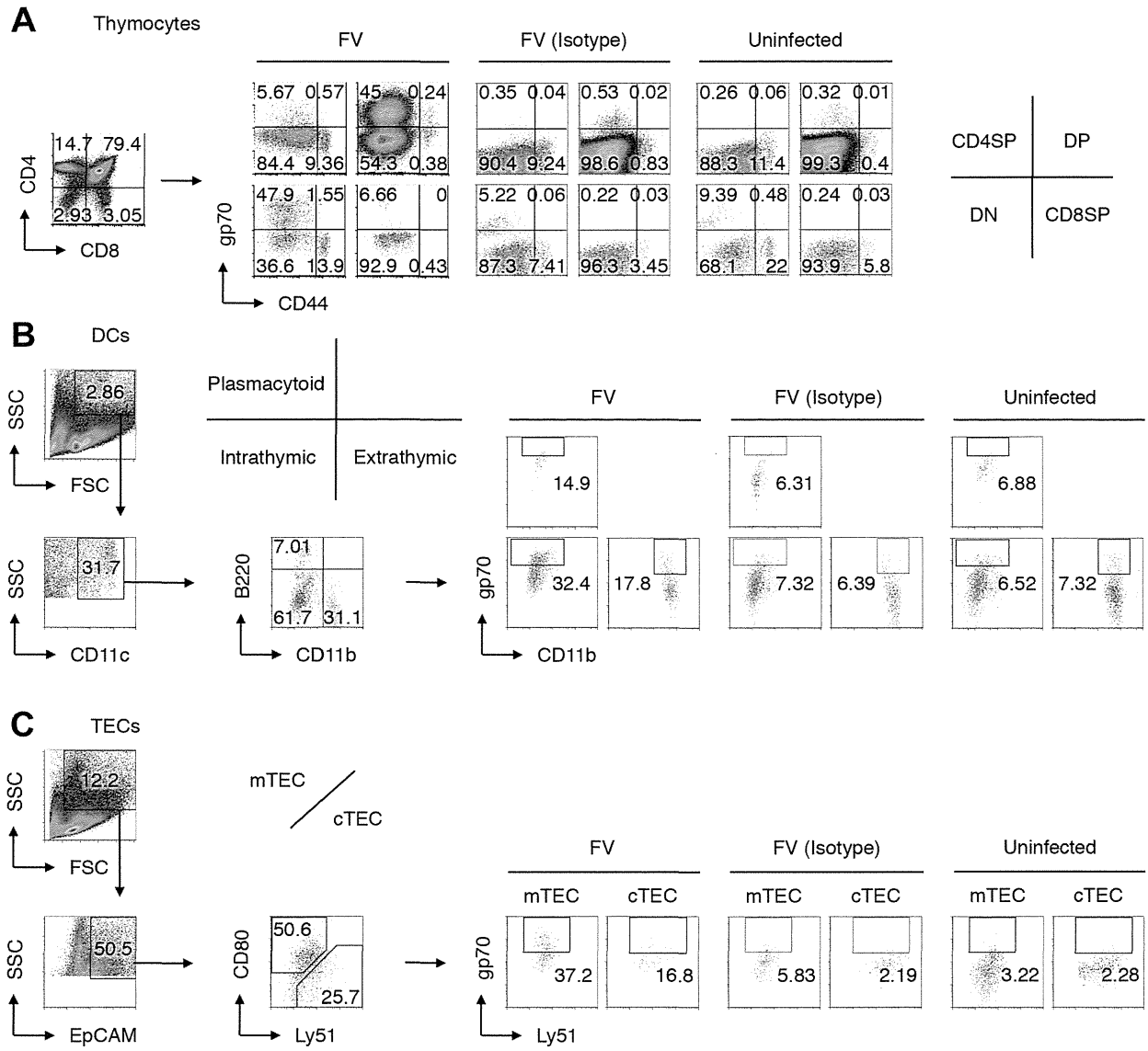

Figure 2. Viral antigen expression in each cell population in the thymus after FV infection. Mice were infected with 1,000 SFFU of FV. At day 14 after infection, cells in the thymus were isolated and stained with indicated Abs. Shown are representative staining patterns and gating protocols of thymocytes (A), thymic DCs (B), and TEC populations (C). (B) Cells purified from the thymus were incubated with microbeads-labeled anti-CD90.2 antibody, and antibody-negative populations were further stained with fluorescent-labeled anti-CD11b, anti-CD11c, anti-B220, and anti-gp70. CD11c$^+$ cells were separated into B220$^+$ plasmacytoid DCs, B220$^-$CD11b$^-$ DCs of intrathymic origin, and CD11b$^+$ DCs of extrathymic origin. (C) CD90.2$^-$ populations were stained with fluorescent-labeled anti-EpCAM, anti-CD80, anti-Ly51, and anti-gp70. EpCAM$^+$ cells were separated into CD80$^+$ medullary TECs (mTECs), and Ly51$^+$ cortical TECs (cTECs). Nonspecific binding of the biotinylated anti-gp70 mAb 720 especially onto DN thymocytes, DCs and TECs was inevitable even in the presence of anti-Fc receptor Abs, as evidenced by the background staining with the isotype control IgG. Thus, the percentages of "gp70$^+$" cells shown here include some background values.
doi:10.1371/journal.ppat.1003937.g002

the DN population among thymocytes also supports this idea (Figure 3D). The expression of FV antigens was also found on the surfaces of all thymic DC populations as well as on medullary (mTECs) and cortical thymic epithelial cells (cTECs) (Figure 2B, C, Figure 3A, C, and Figure S3). Unlike the virus-infected thymocytes, however, the production of infectious virus particles was not detected from the thymic DC and TEC populations, at least by infectious center assays (Figure 3D). These results suggest that although cell-bound viral antigens are detectable in most cell types in the thymus, productive viral replication occurs preferentially in the thymocytes.

Infection of the thymus with FV leads to clonal deletion of FV-specific thymocytes

Given the global nature of FV infection in the thymus, we anticipated that the general function of the thymus in FV-infected mice might be affected. Unlike the spleen, where the physiological architecture was significantly disrupted by the massive expansion of erythroblasts, the vigorous viral replication had no impact on the size of the thymus (data not shown), and caused no apparent morphologic abnormality even at the peak of infection (Figure 4A). The frequencies and absolute numbers of each thymocyte population in FV-infected mice were also not different from those

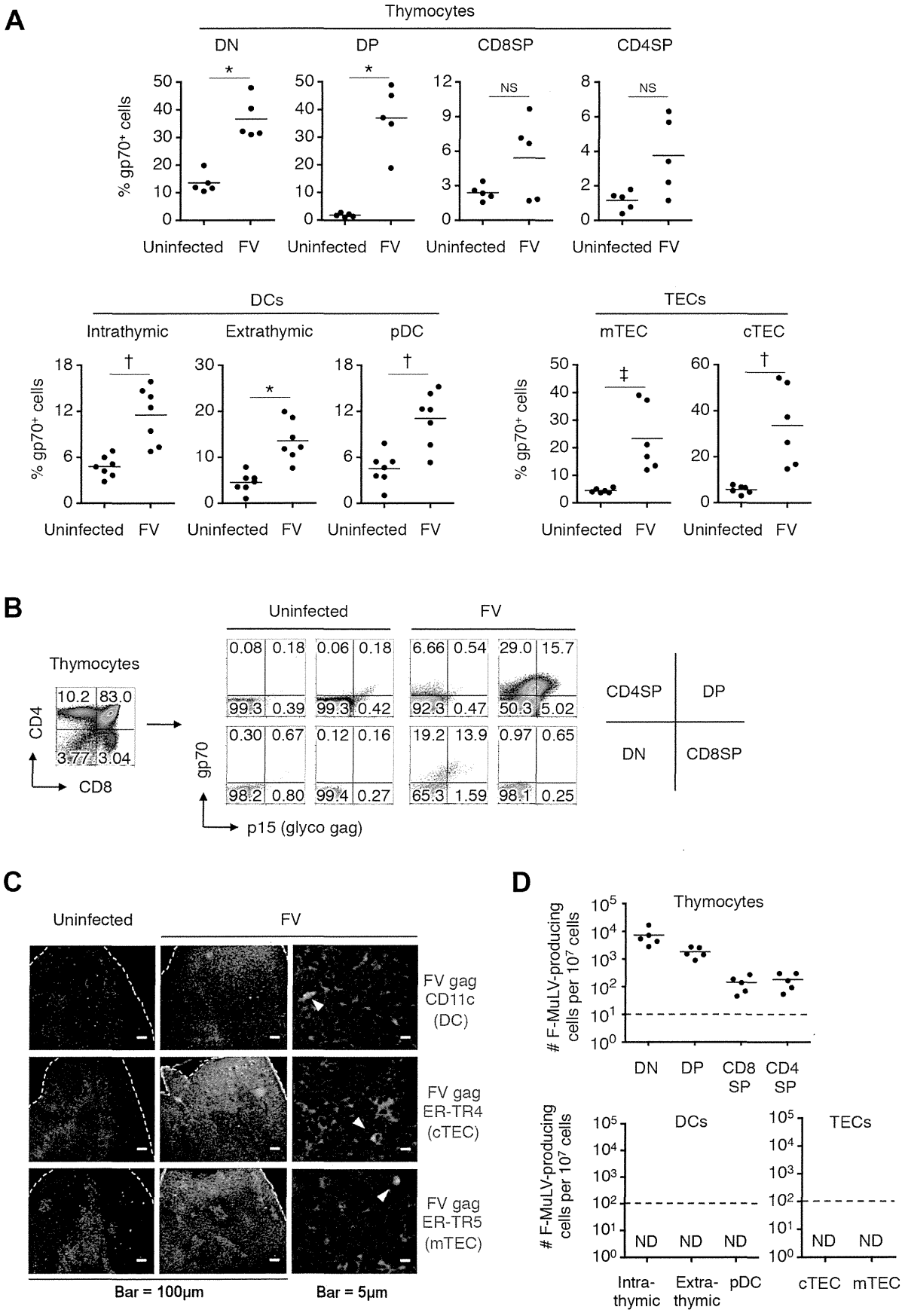
A
Thymocytes
DN
DP
CD8SP
CD4SP
% gp70+ cells
Uninfected
FV
NS
DCs
Intrathymic
Extrathymic
pDC
TECs
mTEC
cTEC
B
Thymocytes
CD4
CD8
Uninfected
FV
gp70
p15 (glyco gag)
CD4SP
DP
DN
CD8SP
C
Uninfected
FV
FV gag CD11c (DC)
FV gag ER-TR4 (cTEC)
FV gag ER-TR5 (mTEC)
Bar = 100μm
Bar = 5μm
D
Thymocytes
F-MuLV-producing cells per 10^7 cells
DN
DP
CD8 SP
CD4 SP
DCs
TECs
ND
Intra-thymic
Extra-thymic
pDC
cTEC
mTEC